#### POLITECNICO DI TORINO

Department of Mechanical and Aerospace Engineering (DIMEAS)



**Master Thesis** 

## Modelling of a Thermocline Thermal Energy Storage System Equipped with 3 Serpentines

#### **Supervisors**

Prof. Roberto Bonifetto (Academic Supervisor)
Dr. Mattia Cagnoli (External Supervisor-ENEA)
Dr. Mehdi Shokrnia (External teaching staff)

#### Host Company

Italian National Agency for New Technologies, Energy and Sustainable Economic Development - ENEA

### Candidate Ali Mahmoudi (316523)



NEMOLAb
(Nuclear Engineering Modeling Laboratory)

October 2025

#### **Dedication**

To my dearest family,

You are the reason behind every step I take and every dream I pursue.

You have stood beside me with love, faith, and endless support.

Everything I have is yours.

#### Acknowledgement

I would like to express my sincere gratitude to my supervisors Prof. Bonifetto, Dr. Cagnoli and Dr. Shokrnia for their invaluable guidance, continuous support, and encouragement throughout this research.

I am also deeply grateful to the Italian National Agency for New Technologies, Energy and Sustainable Economic Development (ENEA) and the Nuclear Engineering Modeling Laboratory (NEMOLab) for hosting my research and providing the resources and environment that made this work possible.

My heartfelt thanks go to my family for their endless love, patience, and unwavering belief in me, and to my friends for their support and companionship throughout this journey.

To all who contributed directly or indirectly to this thesis, I extend my deepest appreciation.

Modelling of a thermocline thermal energy storage system equipped with 3 serpentines.

#### **Abstract**

Hybrid solar plants that combine concentrated solar power (CSP) and photovoltaic (PV) technologies require efficient thermal energy storage (TES) to ensure continuous and flexible operation. This work was carried out within the framework of an ongoing project supported by the Italian National Agency for New Technologies, Energy, and Sustainable Economic Development (ENEA).

Thermocline single-tank systems are a promising solution because of their compactness and cost advantages, but their performance strongly depends on how effectively the thermocline can be maintained during charging and discharging. In this thesis, a computational fluid dynamics (CFD) model of a thermocline TES tank with three internal serpentine coils is developed. The system is examined under different charging compositions: CSP-only, PV-only, balanced CSP-PV input, and simultaneous CSP-PV charging at high power. The results show that the time required to reach a target outlet temperature varies across scenarios, yet the thermocline shape remains broadly similar in all cases, and its quality is not satisfactory. To improve thermal stratification, orifices were introduced inside the charging/discharging channel. Several parameters were investigated, including their position, radius, and number. The study finds that while the position of orifices has little impact, increasing the number of orifices and reducing their radius significantly enhances the sharpness of the thermocline and delays its degradation. Overall, the study highlights that while the composition of CSP and PV inputs mainly affects charging time rather than thermocline shape, the integration of channel orifices provides a practical and effective way to improve stratification quality. These findings offer valuable guidance for the design of advanced TES systems to support flexible operation in hybrid solar plants.

Keywords: Concentrated Solar Power (CSP), Photovoltaic (PV), Hybrid Solar Plants, Thermocline Thermal Energy Storage, Computational Fluid Dynamics (CFD), Orifice Optimization

#### **List of Content**

Chapter 1 – Introduction & Review of Literature	1
1.1 Background and Motivation	2
1.2 Research Gap and Objective	3
1.3 Thermocline Thermal Energy Storage: Operating Principles	3
1.4 Role of Internal Serpentines in Stratification Control	4
1.5 Research Approach	4
1.6 Advancements in Thermocline TES Design	5
1.7 Multi-Serpentine Configurations for Hybrid Integration	5
1.8 Numerical Modeling Considerations	6
1.9 Challenges in Multi-Source Charging and Discharging	6
1.10 Control Strategies for Preserving Stratification	7
1.11 Significance of This Study	7
1.12 Broader Context: Hybrid Renewable Energy Systems	8
1.13 Technological Relevance of 3-Serpentine TES	8
1.14 Structure of the Thesis	9
Chapter 2 – Theoretical Background	10
2.1 Heat Transfer in TES Systems	11
2.1.1 Conduction Heat Transfer in TES Systems	
2.1.2 Convection Heat Transfer in TES Systems	
2.1.3 Heat Transfer in Molten Salts and Liquid Thermal Media	
2.2 Buoyancy-Driven Flows and Thermocline Formation	14
2.2.1 Mixing and Thermocline Degradation Mechanisms	
2.2.2 Effect of Orifices on Flow Distribution in Channels	
2.3 Governing Equations for Thermal-Fluid Modelling	18
2.3.1 Continuity Equation	
2.3.2 Momentum Equation (Navier-Stokes Equations)	
2.3.3 Energy Equation	

2.3.4 Darcy-Forchheimer Law for Porous Media Flow	
2.3.5 Simplifications for TES Modelling	
2.4 Summary and Relevance to Multi-Serpentine TES	21
Chapter 3 – Methodology & Model Setup	22
3.1 Modelling Framework	23
3.2 Computational Domain and Geometry	24
3.2.1 Storage Tank	
3.2.2 Serpentine Heat Exchangers	
3.2.3 Symmetric Approximation	
3.2.4 Domain Boundaries	
3.3 Material Properties	29
3.3.1 Heat Storage Medium	
3.3.2 Porous Media Representation of Serpentines	
3.4 Physics Models and Governing Assumptions	31
3.4.1 Flow Assumptions – Laminar Regime	
3.4.2 Heat Transfer Modelling	
3.4.3 Numerical Simplifications	
3.5 Initial Conditions	33
3.6 Numerical Setup and Discretization	33
3.6.1 Mesh Generation	
3.6.2 Grid Independence Study	
3.6.3 Time-Step Sensitivity	
3.6.4 Inner Iteration Sensitivity	
3.6.5 Solver Settings and Implemented Models	
3.7 Simulation Scenarios	40
3.7.1 Scenarios Based on Inlet Power Composition	
3.7.2 Effect of Orifices on PV/CSP Channels	
3.7.3 Evaluation Criteria	

Chapter 4 – Results & Discussion	43
4.1 Overview of the Simulation Process	44
4.2 Effect of Inlet Power Composition on Thermocline Formation	44
4.2.1 Temperature Evolution	
4.2.2 Temperature–Time Behavior	
4.2.3 Velocity Field Analysis	
4.2.4 Vertical Temperature Distribution	
4.3 Effect of Orifices on Thermal Stratification	52
4.3.1 Influence of Orifice Position	
4.3.2 Influence of Orifice Radius	
4.3.3 Influence of Number of Orifices	
4.3.4 Comparison with Reference Case	
4.4 Discussion	58
Chapter 5 – Conclusion	60
5.1 Summary of the Work	61
5.2 Key Results and Findings	61
5.3 Recommendations and Future Work	63
References	64

#### **List of Figures**

Figure 1 – Hybrid CSP/PV Plant	2
Figure 2 – The Computational Domain	25
Figure 3 – Configuration of Charging and Discharging Serpentines	26
Figure 4 – Approximation of the Coil–Fluid Interaction with Porous Region	27
Figure 5 – Boundary Conditions	28
Figure 6 – Mesh Generation and Prism Layers	34
Figure 7 – Mesh Quality	35
Figure 8 – Grid Independence Study Graph: Temperature vs Number of Cells and Mass	36
Flow Rate vs Number of Cells	
Figure 9 – Time-Step Sensitivity Graph: Temperature vs Time Step and Mass Flow Rate	37
vs Time Step	
Figure 10 – Inner Iteration Sensitivity Graph: Temperature vs Inner Iteration and Mass	39
Flow Rate vs Inner Iteration	
Figure 11 – Temperature Contour for Different Charging Scenarios	45
Figure 12 – Temperature vs Time for Different Charging Scenarios	49
Figure 13 – Velocity Contour for Different Charging Scenarios	50
Figure 14 – Thermocline Formation for Different Charging Scenarios	52
Figure 15 – The Geometry of Orifices	52
Figure 16 - Numerical Simulation Contours after 900 s of Charging in Presence of	54
Orifices	
Figure 17 – Effect of Orifice Position	55
Figure 18 – Effect of Orifice Radius	56
Figure 19 – Effect of Number of Orifices	57

#### **List of Tables**

Table 1 – Grid Independence Study	35
Table 2 – Time-Step Sensitivity	37
Table 3 – Inner Iteration Sensitivity	38
Table 4 – Different Charging Scenarios	45
Table 5 – Simulated Cases to Analyze the Effects of Position, Radius, and Number of	53
Orifices	

# Chapter 1 Introduction



#### 1.1 Background and Motivation

In the face of accelerating climate change, the transition toward renewable energy systems has become a defining challenge for the global energy sector. Among the available renewable resources, concentrated solar power (CSP) provides dispatchable thermal energy that can be efficiently stored and later converted into electricity. Because solar radiation is intermittent, thermal energy storage (TES) is a fundamental component of modern CSP plant design, a point established both by recent reviews and by early CSP development work on advanced TES for parabolic trough systems [1,5].

Among the TES options, thermocline single-tank systems have gained attention for their compactness, reduced capital cost, and the potential to maintain stratification over repeated charge–discharge cycles [1]. These systems operate via sensible heat storage: natural density differences in the molten salt form a thermocline layer that separates hot and cold regions during operation.

Despite these advantages, thermocline tanks face challenges of thermal mixing, heat loss, and stratification degradation, especially over long or cyclic operation. To mitigate these issues, researchers have explored internal heat exchangers to enhance heat transfer while limiting disturbance of the stratified layers. Recent studies consider multiple internal serpentines to separate charging and discharging paths and guide internal flow, improving temperature uniformity and control over the thermal gradient [2].

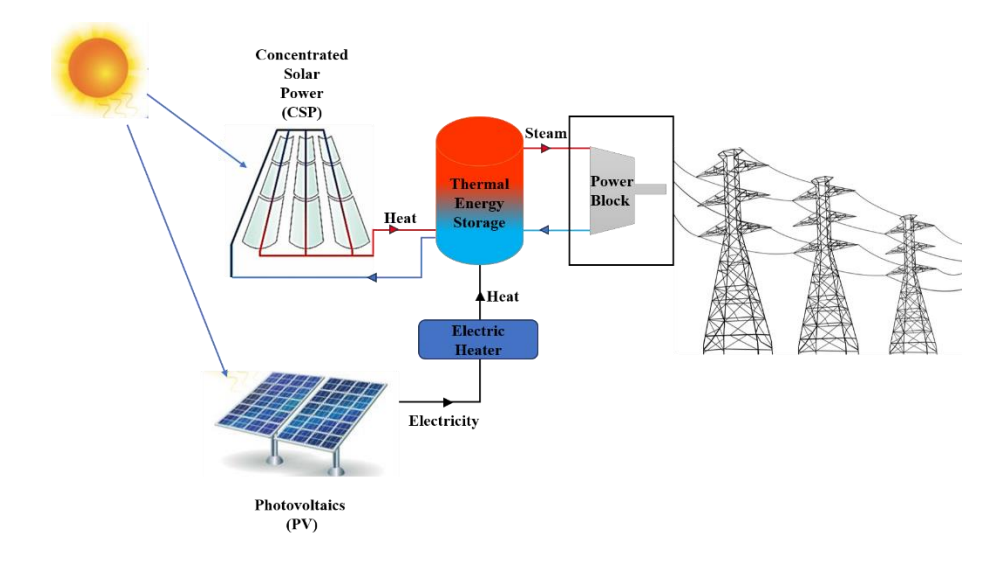


Figure 1 - Hybrid CSP/PV plant

When thermocline TES is integrated in hybrid CSP-PV plants, the system must handle variable charging inputs, calling for flexible thermal management strategies to avoid overheating or inefficiency [3,4].

#### 1.2 Research Gap and Objective

While many numerical and experimental studies have investigated single-coil or shell-and-tube configurations in TES tanks, the performance of a system with three distinct internal serpentines remains largely unexplored. Adding a third serpentine introduces new thermal—fluid interactions that may improve controllability or performance but can also create recirculation zones or non-uniform stratification, as suggested by prior work on coil effects [2].

The aim of this work is to numerically model a thermocline TES tank equipped with three internal serpentines, analyzing its thermal behavior, flow distribution, and stratification quality under various operating conditions. By simulating this configuration, the study seeks to identify design parameters that optimize thermal efficiency and charging performance in hybrid CSP–PV contexts, building on both contemporary TES reviews and foundational CSP TES developments [1,5].

#### 1.3 Thermocline Thermal Energy Storage: Operating Principles

A thermocline TES tank typically consists of a single, well-insulated vessel filled with a heat storage medium such as molten salts, thermal oils, or water. Heat exchangers are strategically positioned to enable both charging and discharging operations. During charging, hot fluid enters through an inlet near the bottom of the tank, pushing the thermal front upward through the storage medium. The thermocline acts as a buffer zone, maintaining a steep temperature gradient between the hot and cold regions. During discharging, the flow direction reverses, and the stored thermal energy is extracted for use in the power cycle or load.

Key performance indicators for thermocline systems include:

- Thermocline thickness, which represents stratification quality
- Energy efficiency, the ratio of recovered to stored thermal energy

• Thermal losses, which quantify heat dissipation through the tank walls, connections, and internal structures.

Maintaining a thin thermocline is essential for maximizing exergy and minimizing mixing losses. Poorly designed internal flow paths or strong buoyant currents can lead to plume formation and diffusion, causing premature mixing and lower outlet temperatures during discharge [6,9].

#### 1.4 Role of Internal Serpentines in Stratification Control

Internal serpentines, helically coiled heat exchangers, are often employed to transfer heat between the heat transfer fluid (HTF) and the storage medium in indirect TES systems. Their number, geometry, and placement significantly influence internal flow distribution, mixing intensity, and heat transfer performance [7]. The presence of multiple coils enables localized heat release or extraction, helping to control the thermocline position and stability throughout charging and discharging processes.

To better understand these interactions, computational fluid dynamics (CFD) has become a powerful tool for visualizing internal flow patterns, predicting temperature fields, and optimizing system design before experimental prototyping [8]. CFD analyses can capture buoyancy effects, temperature-dependent material properties, and transient flow development, providing valuable insight into how coil configuration or flow control strategies affect overall stratification [10].

#### 1.5 Research Approach

In this work, a three-serpentine thermocline TES configuration is numerically modeled to evaluate its thermal performance and flow characteristics. The analysis focuses on:

- Quantifying charging performance under different inlet power scenarios
- Assessing stratification quality when multiple charging sources operate simultaneously or sequentially
- Evaluating thermal efficiency and temperature uniformity for the proposed design

The modeling framework employs CFD simulations for the molten-salt domain, coupled with appropriate boundary conditions representing the internal serpentines. The numerical model incorporates realistic thermophysical properties and operational constraints to reproduce practical conditions. This approach allows for a parametric investigation of different charging compositions and the impact of introducing orifices along the channels on the thermocline shape and stability.

#### 1.6 Advancements in Thermocline TES Design

Over the past decade, extensive research has sought to enhance the thermal performance and reliability of thermocline TES systems. Improvements have focused on several design aspects:

- Tank geometry optimization to minimize stagnant regions and maximize the active storage volume
- Advanced insulation strategies to reduce conductive and radiative losses
- Inlet and outlet flow-diffuser designs to suppress mixing and maintain stratification under high flow rates
- Integration of latent-heat materials within or near the thermocline region to extend operational stability [11].

In hybrid CSP–PV systems, such innovations are especially valuable because charging profiles can vary significantly with weather conditions, solar-field layout, and instantaneous power demand. Efficient TES operation requires flexible control capable of handling partial loads, fluctuating inlet temperatures, and simultaneous charging from multiple sources [12].

#### 1.7 Multi-Serpentine Configurations for Hybrid Integration

Conventional thermocline tanks generally employ a single or dual heat exchanger, but recent studies have explored multi-serpentine configurations to divide the tank into functional thermal zones. In such designs:

- One serpentine may serve high-temperature charging from the CSP loop
- Another may manage mid-temperature charging from a PV-powered electric heater

• A third may be assigned to low-grade or auxiliary heating duties such as waste-heat recovery [13].

This spatial separation of functions allows optimized flow paths for each energy source, reducing thermal interference. However, the coexistence of multiple thermal fronts within the same tank can produce complex flow recirculation patterns and local mixing. For this reason, computational fluid dynamics (CFD) modeling is indispensable for predicting temperature evolution and verifying the stability of stratification [14].

#### 1.8 Numerical Modeling Considerations

Numerical analyses of thermocline TES systems require meticulous attention to several modeling factors:

- Appropriate turbulence treatment for buoyancy-driven flows
- Accurate representation of temperature-dependent thermophysical properties of molten salts
- Grid-independence and time-step sensitivity assessments to guarantee numerical stability and convergence accuracy.

Following these practices ensures reliable predictions and enables exploration of multiple operational scenarios, such as varying charging sequences or hybrid-source configurations, before committing to large-scale prototype development [15].

#### 1.9 Challenges in Multi-Source Charging and Discharging

Operating a thermocline TES tank with multiple charging and discharging sources introduces several engineering challenges. Thermal-front interference may occur when heat is injected at different heights or from different serpentines at the same time, causing the fronts to merge or distort and reducing the outlet temperature sooner than expected. Flow short-circuiting, in which heated fluid bypasses the thermocline region, can drastically diminish usable capacity. In addition,

non-uniform temperature gradients along the serpentines can decrease local heat-transfer effectiveness and promote material degradation through thermal-stress cycling [16].

Therefore, multi-source TES design and operation must balance thermal performance with mechanical reliability, ensuring consistent, high-quality thermal output under variable operating conditions.

#### 1.10 Control Strategies for Preserving Stratification

To mitigate these challenges, researchers have proposed flow-control strategies that dynamically adjust charging and discharging behavior based on real-time temperature feedback. Typical approaches include:

- Variable-flow-rate control to slow thermocline movement and reduce mixing
- Sequential charging from different serpentines to prevent simultaneous thermal-front interaction
- Bypass-flow diversion to stabilize temperature distribution in critical regions of the tank
   [17]

Such control concepts can be implemented using automated valve systems or adjustable-speed circulation devices integrated with supervisory plant control, allowing optimized thermal management in hybrid CSP–PV operation.

#### 1.11 Significance of This Study

This research contributes to the field of solar-thermal energy storage by:

- 1. Providing a detailed CFD-based performance assessment of a thermocline TES tank equipped with three internal serpentines.
- 2. Examining charging, discharging, and hybrid operating scenarios to identify strategies for maximizing thermal efficiency.

- 3. Proposing design and control recommendations relevant to hybrid renewable energy integration.
- 4. Introducing orifices within the channels as a passive means to enhance heat distribution and stratification performance.

The outcomes of this work are expected to offer practical guidance for system designers and operators of hybrid CSP-PV plants seeking improved reliability, higher renewable penetration, and greater dispatchability.

#### 1.12 Broader Context: Hybrid Renewable Energy Systems

The ongoing transition toward high renewable-energy penetration is driving the development of hybrid power plants that integrate multiple renewable sources with flexible energy-storage technologies. Among these, CSP/PV hybrid systems are particularly promising because they combine low-cost electricity generation from PV with dispatchable thermal power from CSP. In such systems, the thermocline TES tank acts as a central thermal hub, enabling excess PV electricity to be converted into heat via electric heaters, while CSP heat can be stored directly through high-temperature molten-salt loops [21].

This hybrid configuration increases operational flexibility and plant dispatchability, allowing stable power delivery even under fluctuating solar-irradiance conditions [22–24].

#### 1.13 Technological Relevance of 3-Serpentine TES

A three-serpentine TES design offers several potential advantages over conventional single- or dual-coil systems:

- Dedicated charging and discharging loops for different energy sources or thermal sinks.
- The ability to isolate thermal fronts, maintaining stratification quality over extended operation.
- Enhanced operational flexibility to adapt to varying resource availability and market demand.

Despite these theoretical benefits, no comprehensive CFD study has yet quantified the detailed thermofluidic behavior of such a configuration under realistic operating conditions. This is particularly relevant for molten-salt TES operating between 200 °C and 600 °C, where buoyancy-driven convection, heat-transfer effectiveness, and material durability strongly influence performance. Addressing this research gap is the main focus of the present study [25].

#### 1.14 Structure of the Thesis

The remainder of this thesis is organized as follows:

- Chapter 2 presents the theoretical background of thermocline TES operation, including governing equations, convection and conduction fundamentals, and heat-exchanger performance principles.
- Chapter 3 describes the numerical-modeling methodology, computational domain, material properties, boundary conditions, and validation procedures.
- Chapter 4 reports and discusses the simulation results.
- Chapter 5 summarizes the conclusions and outlines recommendations for future work.

Through this structure, the thesis provides both scientific understanding and practical design guidance for multi-serpentine thermocline TES systems used in hybrid solar-energy applications.

# Chapter 2 Theoretical Background

#### 2.1 Heat Transfer in TES Systems

#### 2.1.1 Conduction Heat Transfer in TES Systems

Conduction is the most fundamental mode of heat transfer in thermal energy storage (TES) systems and plays a central role in defining the thermal response of both the storage medium and the tank structure. It is governed by Fourier's law of heat conduction, which states that the rate of heat transfer through a material is proportional to the negative gradient of temperature and the thermal conductivity of the medium. In TES applications, conduction occurs within the solid walls of the tank, the serpentine heat exchangers, and, to a smaller extent, within the storage medium itself when fluid motion is minimal.

In molten salt thermocline systems, conduction becomes particularly significant in regions where fluid velocity is low, such as near the walls of the tank or in stagnant layers of the storage medium. Here, the thermal gradient between hot and cold layers is primarily dissipated by molecular diffusion of heat. Although conduction is typically less effective than convection in transferring energy in fluids, it is the dominant mechanism in establishing and smoothing the temperature stratification zone called the thermocline. A sharper thermocline corresponds to reduced conductive heat leakage between hot and cold regions, resulting in higher exergy efficiency during discharging [26].

The thermal conductivity of the heat storage medium (HSM) is therefore a critical design parameter. For instance, nitrate-based molten salts such as solar salt exhibit relatively low thermal conductivity which limits conductive heat transfer and helps preserve stratification [27]. By contrast, solid fillers or phase-change materials (PCMs) integrated into thermocline systems often display higher thermal conductivity, which accelerates heat diffusion but can also degrade stratification quality if not managed properly [28].

Conduction is also vital in the metallic components of TES systems. Serpentine tubes made of stainless steel or alloys conduct heat from the heat transfer fluid (HTF) to the molten salt medium. The efficiency of this process depends on both the conductivity of the tube material and the thickness of the tube wall. Thinner, high-conductivity materials enable faster thermal response but may raise concerns about structural durability at high operating temperatures [29]. Similarly, conduction through the insulating layers of the tank walls defines the overall thermal losses to the

environment. High-performance insulation materials with low conductivity, such as ceramic fiber blankets or aerogels, are typically used to minimize heat leakage during long-duration storage [30].

In summary, while conduction alone is rarely sufficient to transport large quantities of energy in TES systems, it plays a decisive role in shaping the thermocline, governing material heat transfer, and determining insulation effectiveness. Its interaction with convection ultimately dictates the overall performance of multi-serpentine thermocline tanks.

#### 2.1.2 Convection Heat Transfer in TES Systems

Convection is the dominant mechanism of heat transfer in liquid-based thermal energy storage (TES) systems, particularly in thermocline tanks where large volumes of molten salt are used. It involves the bulk motion of the fluid caused by buoyancy force, which drive the vertical circulation of the molten salt and govern the formation and evolution of the thermocline.

When heat is introduced into the tank, the fluid in contact with the heated surfaces becomes less dense and rises, while the colder, denser fluid descends, establishing buoyancy-driven circulation loops. This natural convection process plays a decisive role in shaping the thermocline, the transitional region that separates the hot and cold fluid layers. The characteristics of this layer, such as its thickness and stability, directly determine the quality of energy storage and retrieval.

The intensity of natural convection depends on several factors, including the temperature gradient, fluid viscosity, thermal expansion coefficient, and specific heat capacity of the molten salt. A moderate temperature difference promotes smooth and stable stratification, while larger gradients can induce stronger convective motion and undesirable mixing, which leads to a gradual broadening of the thermocline [31].

Geometrical aspects of the tank also influence convective behavior. Taller tanks tend to promote stronger buoyant motion due to greater hydrostatic head, while proper insulation of the sidewalls minimizes lateral heat losses that could disturb vertical stratification. Inlet configuration and flow distribution features, such as internal diffusers or orifices, can further modify the circulation patterns and help sustain a stable thermocline over repeated charging cycles [32].

The efficiency of heat transfer associated with natural convection is often described by the Nusselt number (Nu), which expresses the ratio of convective to conductive heat transfer within the fluid. In laminar buoyant flow, this value depends strongly on the Rayleigh number (Ra), which characterizes the balance between buoyancy and viscous forces [33]. Analytical and numerical studies have shown that increasing the Rayleigh number enhances heat transfer but can also accelerate thermocline degradation [34].

Overall, natural convection governs the heat transport and stratification behavior within thermocline TES systems. Its control through tank geometry, material properties, and inlet design is crucial to maintaining a sharp temperature gradient and achieving high thermal storage performance [35].

#### 2.1.3 Heat Transfer in Molten Salts and Liquid Thermal Media

The choice of heat storage medium (HSM) is one of the most critical aspects in designing efficient thermocline thermal energy storage (TES) systems. Liquids are particularly attractive for TES because they provide continuous phase operation, simple tank construction, and relatively stable thermophysical properties across a wide temperature range. Among them, molten salts have become the most widely used high-temperature medium due to their favorable combination of heat capacity, stability, and cost-effectiveness.

Molten salts are capable of storing large amounts of thermal energy between approximately 290°C and 565°C. Their relatively high specific heat capacity, around  $1.5 \, kJ/kg \cdot K$ , allows significant energy to be stored in modest volumes, while their low vapor pressure makes them suitable for atmospheric-pressure operation, reducing tank design complexity [36]. However, their thermal conductivity is relatively low, around  $0.5 \, W/m \cdot K$ , which helps preserve stratification by limiting conductive heat leakage but simultaneously limits the rate of local heat transfer [37].

Alternative liquid storage media have also been investigated. Synthetic thermal oils can operate at lower temperatures, up to 400°C, and offer good thermal stability at moderate conditions, making them suitable for hybrid solar and industrial heating systems. However, they degrade chemically at higher temperatures and typically have lower heat storage density than molten salts [38]. Liquid metals such as sodium and lead-bismuth alloys have been considered in research settings for their

extremely high thermal conductivity and ability to sustain very high operating temperatures. Despite their superior heat transfer properties, their cost, corrosion issues, and safety concerns make them less attractive for large-scale TES applications [39].

The performance of molten salt-based TES is not governed solely by material properties but also by flow behavior inside the tank. In multi-serpentine configurations, molten salt interacts with coiled heat exchangers, where heat transfer occurs primarily through convection, but conduction within stagnant zones remains important. Recent CFD studies have highlighted that the viscosity-temperature dependence of molten salts is a crucial factor, as temperature decreases, viscosity rises sharply, slowing down convection currents and thereby enhancing the role of conduction in stratification maintenance [40].

In practical applications, impurities and repeated cycling can also affect the thermophysical properties of molten salts. Decomposition of nitrates at elevated temperatures releases oxygen and nitrogen oxides, potentially changing both thermal conductivity and specific heat over time. Continuous monitoring and periodic salt purification are therefore required to ensure reliable and predictable heat transfer performance in long-term operation.

In brief, molten salts represent the best compromise between cost, thermal performance, and stability for thermocline TES systems operating in the 300-600°C range. Their heat transfer behavior reflects a balance between conduction in stagnant layers and convection in active flow regions, with system-level performance highly dependent on operating conditions and coil design.

#### 2.2 Buoyancy-Driven Flows and Thermocline Formation

In a thermocline thermal energy storage (TES) tank, buoyancy-driven flows are fundamental to the establishment and maintenance of thermal stratification. These flows arise from density variations in the heat storage medium, typically molten salt, as it undergoes temperature changes. When hotter fluid becomes less dense, it rises, while cooler and denser fluid sinks, creating circulation patterns within the tank. This process, known as natural convection, is the primary mechanism responsible for the vertical temperature gradient that defines the thermocline layer.

The thermocline is a distinct transition zone separating the upper hot region from the lower cold region of the tank. Its thickness and stability determine the quality of stored energy, as a sharp thermocline enables high-temperature discharge for a longer period, while a diffuse or degraded thermocline reduces exergy efficiency. Experimental and numerical studies have shown that buoyancy-driven convection contributes to both the formation and the broadening of the thermocline during repeated charge-discharge cycles [41].

At the onset of charging, heat introduced from serpentine coils or inlet ports drives local buoyancy currents. These currents transport heat upward, establishing a sharp interface between hot and cold zones. However, as charging continues, mixing induced by these flows tends to thicken the thermocline. The rate of thickening depends on fluid properties such as viscosity, thermal diffusivity, and thermal expansion coefficient. For molten salts, relatively high viscosity at lower temperatures helps suppress excessive mixing, which is beneficial for stratification [42].

Several studies have highlighted that the geometry of the tank and inlet configuration strongly affect buoyancy-driven flow patterns. Vertical inlets located at the bottom of the tank enhance upward buoyant plumes that strengthen stratification, while lateral inlets may cause horizontal mixing that erodes the thermocline. Similarly, the arrangement of multiple serpentines influences how thermal plumes interact. In a 3-serpentine system, simultaneous heating from different vertical positions can create interfering buoyancy cells, complicating the stability of the thermal front [43].

Buoyancy-driven flows also play a central role during standby periods, when the tank is neither actively charged nor discharged. Even without forced flows, thermal diffusion at the thermocline generates density gradients that trigger weak convection currents, slowly degrading stratification over time. This phenomenon, often referred to as self-mixing, limits the long-term storage efficiency of single-tank systems. Advanced insulation strategies and optimized coil placement can mitigate this effect by minimizing thermal disturbances [44].

Overall, buoyancy-driven flows represent a double-edged sword. They are essential for establishing the thermocline but also responsible for its eventual degradation. Understanding and controlling these flows through careful design of serpentine configurations, inlet velocities, and operating strategies is therefore critical to maximizing the effectiveness of thermocline TES systems [45].

#### 2.2.1 Mixing and Thermocline Degradation Mechanisms

The effectiveness of a thermocline thermal energy storage (TES) system relies on maintaining a sharp temperature gradient between hot and cold regions of the tank. However, in practice, various forms of mixing gradually degrade this stratification, leading to a thicker thermocline and a corresponding reduction in the quality of stored energy. The ability of the TES system to deliver high-temperature output for extended periods is therefore directly linked to how mixing is understood, minimized, and controlled.

The main categories of mixing have been identified in thermocline tanks are buoyancy-driven mixing and diffusive mixing.

- Buoyancy-driven mixing occurs naturally during standby, when temperature gradients generate weak convective currents that slowly erode the thermocline. This process is unavoidable but progresses more rapidly in tall tanks or when the thermal expansion coefficient of the storage medium is high [46].
- Diffusive mixing, although slower, occurs due to molecular heat conduction across the thermocline. While its contribution is small compared to convective mixing, it becomes significant during long idle periods [47].

The geometry and placement of serpentines strongly influence the severity of mixing. For example, coils positioned too close to the thermocline interface may induce localized turbulence, accelerating stratification breakdown. In multi-serpentine systems, simultaneous operation of multiple coils can generate interacting flow structures, further increasing mixing intensity if not carefully controlled [48].

Recent CFD studies and experimental campaigns have proposed several mitigation strategies. The use of flow diffusers at inlets reduces jet penetration and distributes momentum more evenly, preserving stratification. Similarly, optimized pumping strategies, such as low Reynolds number flow or pulsed inputs, have been shown to minimize mixing while still enabling efficient energy transfer. Hybrid systems can also employ sequential charging protocols, where different serpentines are activated in succession to prevent overlapping thermal plumes [49].

Collectively, mixing is the central challenge to maintaining long-term thermocline stability. While it cannot be entirely eliminated, it can be significantly reduced through careful design of coil placement, flow distribution, and operating strategies. A successful multi-serpentine TES system must therefore balance efficient heat transfer with minimized mixing to maximize exergy efficiency and system lifetime.

#### 2.2.2 Effect of Orifices on Flow Distribution in Channels

Orifices are widely used in fluid systems to control flow distribution, momentum, and mixing. In the context of thermal energy storage (TES) tanks, introducing orifices along the charging or discharging channels is a promising strategy to improve flow uniformity and thereby enhance thermocline stability. The basic principle is that each orifice acts as a secondary injection point, redistributing mass flow and reducing jet penetration, which are common causes of mixing and stratification degradation.

The performance of orifices is influenced by several key parameters: position, number, and radius. Orifices located near the thermocline region can significantly influence buoyancy-driven plumes, guiding hot or cold fluid into desired layers. However, studies indicate that position alone has a limited effect compared with the combined impact of radius and number [50]. Increasing the number of orifices helps spread the momentum of the injected flow across a larger cross-section, thereby reducing localized turbulence and delaying thermocline broadening [51].

The radius of orifices directly controls the velocity of the jet emerging into the tank. Larger diameters allow high-momentum jets, which can penetrate deeply and disturb stratification, while smaller orifices generate weaker, more diffuse jets that support layer stability [52]. Therefore, designs that employ multiple small-radius orifices are generally more effective than those with a single large inlet.

From a hydraulic perspective, orifices also contribute to pressure drop regulation, which influences pump requirements and system efficiency. Optimized orifice geometry can balance thermal and hydraulic performance, ensuring sufficient mixing for heat transfer without destroying the stratified temperature profile [53]. Experimental and numerical investigations in related systems, such as water storage tanks and packed-bed reservoirs, confirm that distributed inlets using orifices

result in sharper thermoclines and improved outlet temperature profiles compared with single-point injection [54].

In summary, the incorporation of orifices inside the charging/discharging channel provides a practical method to mitigate stratification degradation. While their exact positioning has a secondary influence, the increase in number and reduction in radius of orifices are consistently shown to improve thermocline quality, aligning with the design objectives of multi-serpentine TES systems.

#### 2.3 Governing Equations for Thermal-Fluid Modelling

The numerical modelling of thermocline TES systems is based on the fundamental laws of conservation of mass, momentum, and energy, expressed as partial differential equations (PDEs). These equations capture the complex interactions between conduction, convection, and buoyancy-driven flows in molten salts, enabling prediction of thermal stratification and overall system performance.

#### 2.3.1 Continuity Equation

The continuity equation ensures the conservation of mass within the fluid domain. For an incompressible fluid such as molten salt, it takes the simplified form:

$$\nabla \cdot \vec{u} = 0$$
 Eq.1

where  $\vec{u}$  is the velocity vector. This condition enforces that the net volumetric inflow equals the outflow at any point in the domain, a valid assumption given the negligible compressibility of molten salts under TES operating conditions [55].

#### 2.3.2 Momentum Equation (Navier-Stokes Equations)

Momentum conservation is described by the Navier-Stokes equations, which account for viscous, inertial, and pressure forces. For incompressible Newtonian fluids, the general form is:

$$\rho\left(\frac{\partial \vec{u}}{\partial t} + \vec{u}.\nabla \vec{u}\right) = -\nabla p + \mu \nabla^2 \vec{u} + \rho \vec{g} + \vec{F}$$
 Eq.2

where  $\rho$  is fluid density, p is pressure,  $\mu$  is dynamic viscosity,  $\vec{g}$  is the gravitational acceleration vector, and  $\vec{F}$  represents external body forces. In TES applications, buoyancy is introduced through the Boussinesq approximation, where density variations are neglected except in the buoyancy term:

$$\rho(T) = \rho_0 [1 - \beta(T - T_0)]$$
 Eq.3

with  $\beta$  being the thermal expansion coefficient and  $T_0$  a reference temperature [56]. This approximation reduces computational cost while still capturing buoyancy-driven natural convection.

#### 2.3.3 Energy Equation

The conservation of energy governs heat transport by conduction and convection. It is expressed as:

$$\rho c_p \left( \frac{\partial T}{\partial t} + \vec{u} \cdot \nabla T \right) = k \nabla^2 T + Q$$
 Eq.4

where  $c_p$  is specific heat capacity, k thermal conductivity, and Q represents volumetric heat sources. This equation describes how heat is advected by fluid motion, diffused by conduction, and generated by sources such as resistive heating in serpentine coils [57].

#### 2.3.4 Darcy-Forchheimer Law for Porous Media Flow

In many engineering applications, flow through complex geometries, such as tube bundles, packed beds, or heat exchanger coils, can be approximated using the porous media approach. Instead of resolving the detailed geometry, the overall pressure loss is represented by a momentum sink term added to the Navier-Stokes equations. This relationship is expressed by the Darcy-Forchheimer law, which combines viscous and inertial resistance to flow:

$$-\nabla p = \frac{\mu}{k_p} v + \beta \rho v^2$$
 Eq.5

Where  $\nabla p$  is pressure gradient,  $k_p$  is permeability of the porous medium, v is superficial velocity,  $\rho$  is fluid density and  $\beta$  is inertial (Forchheimer) coefficient.

The first term (Darcy term) represents linear viscous losses that dominate at low velocities, while the second term (Forchheimer term) accounts for quadratic inertial effects relevant at higher flow speeds. Together, they describe the total pressure loss through the porous region.

In the context of this study, the porous subdomains representing the serpentines apply this relationship to simulate flow resistance and momentum exchange between the molten salt and the internal heat transfer fluid. Different permeability and inertial coefficients are used for charging and discharging conditions to reproduce realistic flow behavior and thermal performance. [58]

#### 2.3.5 Simplifications for TES Modelling

Several assumptions are commonly applied to make CFD simulations of TES systems computationally feasible:

- The fluid is treated as incompressible.
- Radiation heat transfer is neglected compared to conduction and convection.
- Thermophysical properties are assumed either constant or temperature-dependent.

These simplifications allow for capturing the dominant physics of stratification and mixing without requiring prohibitive computational resources.

To summarize, the governing equations provide a rigorous mathematical framework for analyzing thermocline TES systems. Their implementation within CFD solvers enables detailed exploration of flow-temperature interactions, which is critical for understanding the performance of multi-serpentine configurations [59].

#### 2.4 Summary and Relevance to Multi-Serpentine TES

The discussion in this chapter has outlined the theoretical foundations necessary for understanding and modelling thermocline thermal energy storage (TES) systems. The review began with the mechanisms of conduction and convection, highlighting their complementary roles in shaping the temperature field inside the storage medium. Conduction governs heat transfer within solid boundaries, stagnant fluid layers, and insulating materials, while convection dominates energy transport in the bulk molten salt, directly affecting stratification quality and thermal response.

The chapter further examined buoyancy-driven flows, which are essential for the formation of a thermocline but simultaneously contribute to its gradual degradation through natural circulation and self-mixing. These processes converge in multi-serpentine configurations, where the convection create complex thermal-fluid dynamics that require careful numerical investigation.

Finally, the governing equations of mass, momentum, and energy conservation were introduced, along with modelling simplifications such as the Boussinesq approximation and incompressibility assumption. Together, these provide the mathematical framework for simulating TES behavior under realistic operating conditions.

In the context of a three-serpentine thermocline TES system, the principles reviewed here are particularly relevant. The simultaneous operation of multiple coils introduces competing buoyancy plumes and flow structures, making it challenging to preserve stratification while ensuring high heat transfer efficiency. The insights from this theoretical foundation therefore serve as the basis for the numerical modelling and simulation work presented in the following chapter.

Chapter 3
Methodology
&
Model Setup

#### 3.1 Modelling Framework

The present work is based on computational fluid dynamics (CFD) modelling of a thermocline thermal energy storage (TES) tank equipped with three internal serpentine heat exchangers. CFD was selected as the primary research tool because it allows detailed investigation of the coupled fluid flow, heat transfer, and buoyancy-driven phenomena inside the storage tank, which are difficult to capture experimentally. All CFD simulations were carried out using STAR-CCM+. This software was selected because it provides reliable tools for analyzing fluid flow and heat transfer in complex geometries. The entire simulation process, including model setup, mesh generation, solution, and post-processing, was performed within the STAR-CCM+ environment. By resolving the governing equations for mass, momentum, and energy conservation across the computational domain, CFD provides spatially and temporally resolved predictions of velocity fields, temperature distributions, and stratification quality. The CFD model of the thermocline TES system developed in this work is based on the model presented and validated against experimental data in studies conducted at ENEA, as reported by Cagnoli et al. [60].

The modelling strategy follows a systematic workflow:

- 1. Geometry definition: the storage tank is represented in a simplified but realistic 3D symmetric domain, capturing the essential physical processes while reducing computational cost.
- 2. Mesh generation: the geometry is discretized into computational cells fine enough to resolve steep gradients near the walls and within the thermocline region.
- 3. Physics setup: governing equations are solved under the assumptions of incompressible flow and the Boussinesq approximation for buoyancy. Heat conduction in solids and convection in the molten salt are fully coupled.
- 4. Boundary and initial conditions: heat power is specified for each serpentine to represent charging condition. Thermal losses from the tank walls are modeled through convection.
- 5. Solution procedure: the discretized equations are solved using a finite volume solver with implicit time stepping to ensure numerical stability during transient simulations.

6. Post-processing: temperature and velocity fields are extracted to evaluate stratification and thermocline thickness.

A key element of this framework is the comparative analysis of different configurations. While the main focus is on the three-serpentine arrangement, baseline cases with one and two serpentines are also simulated. This enables direct evaluation of how additional serpentine affect flow distribution, mixing intensity, and overall heat transfer efficiency. Furthermore, parametric variations in inlet heat power and orifices are introduced to identify optimal operating strategies.

The modelling framework is designed to strike a balance between physical accuracy and computational feasibility. For instance, although three-dimensional simulations would capture all geometric details, a 3-dimensional plane symmetric approach is adopted here, consistent with the cylindrical geometry of the tank and serpentines. This simplification reduces computational cost without significantly compromising accuracy, as confirmed by previous validation studies of similar TES systems.

#### 3.2 Computational Domain and Geometry

As shown in Fig.2, the computational domain represents a single-tank thermocline thermal energy storage (TES) system equipped with three internal serpentine heat exchangers. The tank geometry is simplified for numerical modelling but retains the key physical features required to capture stratification, buoyancy effects, and heat transfer interactions between the serpentines and the molten salt.

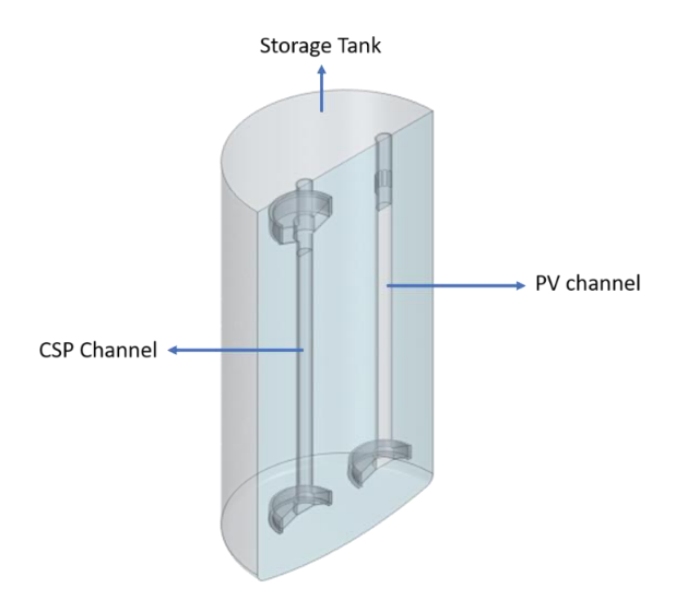


Figure 2 - The computational domain

#### 3.2.1 Storage Tank

The storage tank is modelled as a vertical cylindrical vessel, which is the most common configuration for molten salt TES due to its compact footprint and favorable stratification characteristics. The tank height-to-diameter ratio is chosen to balance storage capacity with thermal stability. The taller tanks promote sharper thermoclines but are more prone to buoyancy-driven mixing, whereas shorter tanks provide more robust mixing but reduce effective energy quality. The inner domain is filled with molten salt, considered the heat storage medium (HSM), while the solid tank walls are not explicitly simulated. Instead, boundary conditions are applied at the domain boundaries to represent heat losses or adiabatic behavior, depending on the scenario [61].

#### 3.2.2 Serpentine Heat Exchangers

The distinguishing feature of this study is the inclusion of three independent serpentine coils, each designed to represent a separate charging or discharging pathway. The serpentines are immersed in the molten salt domain and are geometrically defined as helical or coil-shaped tubes simplified into axisymmetric representations. The fluid flow around the coils totally is considered as porous regions and simulated by considering porous media.

As illustrated in Fig. 3, their relative positions are selected to investigate different modes of operation:

- Upper serpentine: typically connected to the discharging loop, extracting hot fluid from the top region.
- Lower serpentines: connected to charging sources such as CSP or PV-powered heaters, delivering heat to the cold bottom layers.

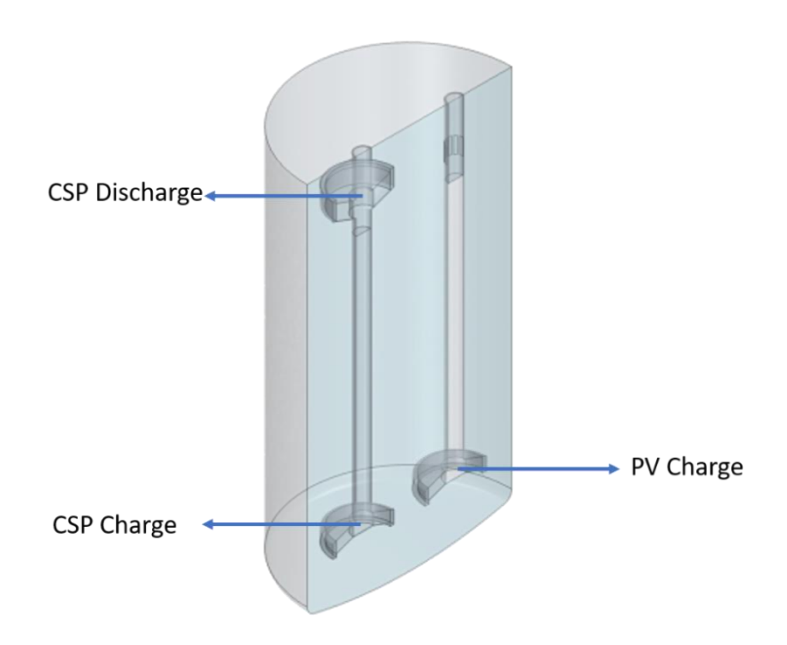


Figure 3 - Configuration of charging and discharging serpentines

The arrangement of three serpentines enables analysis of multi-source charging and segmented discharge strategies, which are not possible in conventional single- or dual-serpentine designs. To reduce computational cost, the serpentine coils are not modelled as explicit helical tubes with fluid domains inside. Instead, the volume they occupy is represented as a porous region embedded in the molten salt domain. This approach approximates the effect of coil-fluid interaction by adding momentum resistance and heat exchange within a porous medium, while avoiding the need to resolve detailed flow inside the narrow serpentine passages.

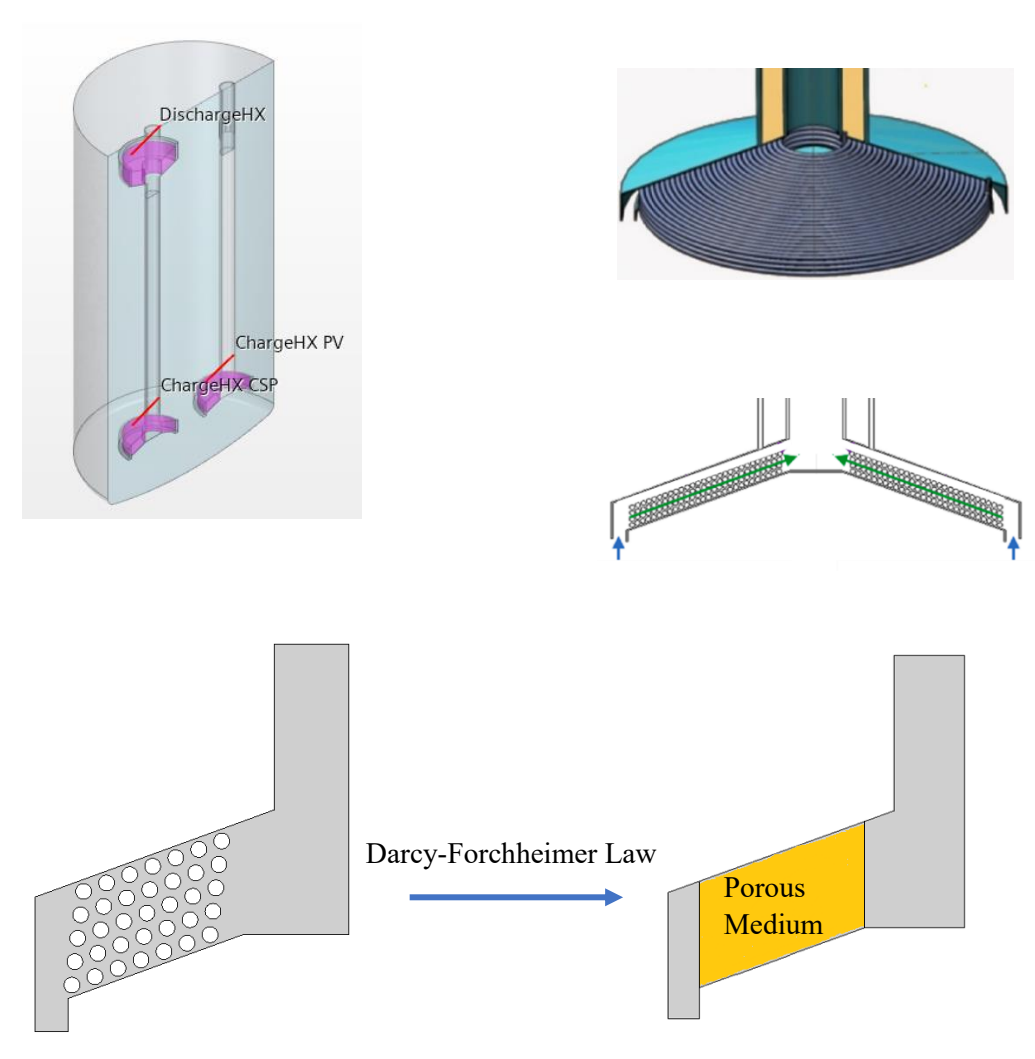


Figure 4 – approximation of the coil-fluid interaction with porous region

#### The porous region approach assumes that:

- Momentum exchange between the heat transfer fluid (HTF) and the molten salt is captured through Darcy-Forchheimer resistance terms, which account for both viscous and inertial losses.
- Heat transfer is imposed via boundary conditions applied on the porous region boundaries, representing the thermal input or output of the coils.
- The geometry of the porous region matches the spatial location of the serpentine bundle, ensuring that buoyancy plumes and convective currents interact realistically with the surrounding molten salt.

This simplification allows accurate prediction of global temperature fields, thermocline evolution, and stratification quality, while significantly reducing mesh size and simulation time compared to fully resolving coil geometries.

# 3.2.3 Symmetric Approximation

The tank is represented as a 3D plane symmetric domain and the serpentine regions are replaced with porous subdomains embedded in the molten salt. This approach reduces computational cost substantially while still capturing the essential flow and thermal interactions.

### 3.2.4 Domain Boundaries

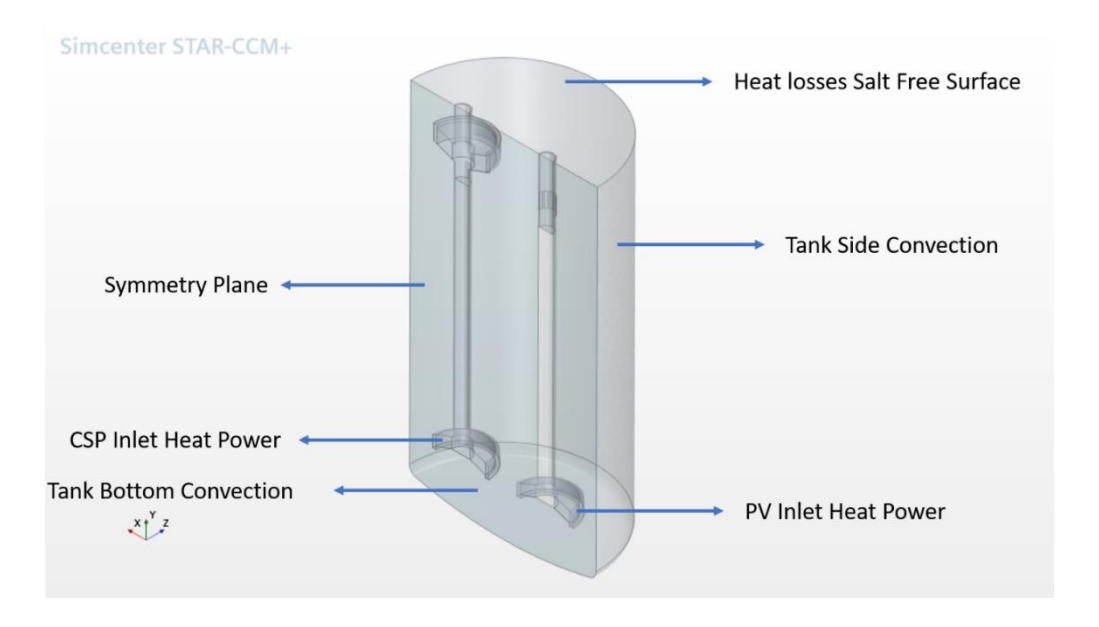


Figure 5 - Boundary Conditions

The domain boundaries are defined as follows:

- Tank walls: Represented as heat loss from the salt free surface and using a prescribed convective heat transfer in the side and bottom of the Tank.
- Serpentine: Applied as constant heat power boundary conditions, varying with the operating scenario (PV only, CSP only, or combined PV/CSP).
- Symmetry Plane: A mid-plane through the tank is considered as a symmetry boundary.

### 3.3 Material Properties

Accurate representation of material properties is essential for predicting the thermal and hydraulic performance of a thermocline TES system. In the present model, two categories of materials are considered: the heat storage medium (HSM) and the serpentine as a porous medium. Each is assigned appropriate thermophysical characteristics to ensure realistic simulation results. The outer walls of the tank are not explicitly modelled as solid layers. Instead, their thermal behavior is approximated through boundary conditions.

### 3.3.1 Heat Storage Medium

The storage medium is modelled as a molten salt mixture, chosen for its high specific heat capacity, moderate thermal conductivity, and ability to operate at elevated temperatures.

Key thermophysical properties of molten salt include:

- Density  $(\rho)$ : An average value is adopted for the density.
- Viscosity (μ): Highly temperature-dependent. viscosity increases at lower temperatures, affecting flow resistance and convective heat transfer. A polynomial function of temperature is therefore used to represent viscosity.
- Specific heat capacity  $(c_n)$ : Determined as a polynomial function of temperature.
- Thermal conductivity (*k*): Relatively low, which restricts conduction and supports thermal stratification.
- Thermal expansion ( $\alpha$ ): Treated as a constant.

# 3.3.2 Porous Media Representation of Serpentines

Instead of explicitly modelling the serpentine coils as solid stainless-steel tubes with thin conductive walls, the heat exchanger regions are represented as porous subdomains within the molten salt. This simplification reduces computational cost and avoids the need to resolve small-

scale coil geometry while still capturing the essential interaction between the heat transfer fluid (HTF) and the storage medium.

The porous media approach introduces additional momentum resistance terms in the Navier-Stokes equations and allows heat exchange to be prescribed volumetrically. Each serpentine region is therefore characterized by hydraulic and thermal parameters that reflect its operating mode (charging or discharging).

The following properties are defined for the porous regions:

- Porous inertial coefficient (charging and discharging): accounts for inertial losses caused by the flow obstruction inside the coil bundle.
- Porous viscous coefficient (charging and discharging): represents viscous drag due to frictional resistance within the porous structure.
- Porous beta factor (charging): regulates the distribution of momentum exchange between the HTF and the molten salt during charging.
- Porous permeability (charging and discharging): controls the ease of fluid passage through the porous zone, affecting both flow resistance and heat transfer.

By tuning the inertial, viscous, and permeability parameters separately for charging and discharging, the porous media model provides a realistic approximation of the hydraulic resistance and thermal interaction that would otherwise occur within the serpentine coils.

Overall, the selected material properties ensure that the simulation accurately captures the interplay of conduction and convection in the molten salt, the thermal role of the serpentines, and the performance of the tank. This provides a realistic foundation for analyzing the operating conditions on thermocline behavior.

# 3.4 Physics Models and Governing Assumptions

The physical processes in a thermocline thermal energy storage (TES) tank are governed by the interaction of buoyancy-driven flows, convection through serpentines, and conductive heat transfer in stagnant fluid zones. To capture these processes, the CFD model implements appropriate physical models while adopting a set of simplifying assumptions to balance accuracy and computational feasibility.

# 3.4.1 Flow Assumptions - Laminar Regime

- The molten salt is treated as an incompressible Newtonian fluid. Density is constant except in the buoyancy term, where the Boussinesq approximation is applied to capture natural convection.
- The flow is transient laminar. All simulations are performed without a turbulence model. This choice is justified by the operating conditions, coil powers and characteristic velocities, yielding Reynolds numbers in the laminar range within both the bulk tank and the porous serpentine regions. In addition, the strong thermal stratification promotes stable, layered motion rather than fully turbulent mixing.
- No-slip is imposed at all solid-fluid interfaces, tank sidewall and bottom. At the top surface,
  a slip velocity boundary is used to approximate the molten-salt/air free surface. Thermal
  losses are applied here via an external heat-transfer coefficient, avoiding explicit
  multiphase modelling.
- The three serpentine zones are represented as porous subdomains. Flow within each porous region is laminar and modelled via Darcy-Forchheimer momentum sources, viscous and inertial resistance.
- Numerical settings like mesh near the thermocline and time step are chosen to minimize numerical diffusion, ensuring the laminar solution preserves the sharpness of the temperature front.

# 3.4.2 Heat Transfer Modelling

- Heat transfer in the molten salt is modelled by solving the energy equation, which accounts for both convective transport, due to bulk motion, and conductive diffusion.
- The serpentines are represented as thermal boundary conditions and constant heat power simulates heat input from CSP or PV
- Heat losses are represented at the salt free surface, while prescribed convective heat transfer coefficients are applied at the side and bottom walls of the tank.

### 3.4.3 Numerical Simplifications

To reduce complexity while preserving essential physics:

- Radiation heat transfer is neglected, as conduction and convection dominate in molten salt
   TES tanks within the studied temperature range.
- As outlined in the material properties section, certain thermal properties of molten salt are implemented as temperature-dependent functions, whereas others are assumed constant over the operating range.
- The computational domain is reduced to a 3D plane symmetric domain of the tank. This captures global stratification behavior while minimizing mesh size and simulation time.

In essence, the chosen physical models and assumptions provide a realistic yet computationally tractable representation of the TES system. They enable the simulation to capture the interplay of conduction and convection from the serpentines, which collectively determine the thermal and hydraulic performance of the three-serpentine configuration.

### 3.5 Initial Conditions

The accuracy of CFD predictions for a thermocline TES system depends strongly on the specification of realistic boundary and initial conditions. These conditions define how heat and mass enter or leave the computational domain, and they establish the initial thermal state of the storage medium before charging begins.

The starting temperature distribution of the molten salt is critical in defining the subsequent evolution of the thermocline. In charging simulations, the tank is initialized at a uniform "cold" reference temperature, and hot fluid is introduced via the charging serpentines.

The reference temperature values for hot and cold zones are chosen according to typical molten salt operating ranges, ensuring consistency with practical applications.

In summary, boundary and initial conditions are formulated to replicate both idealized cases with adiabatic tank and uniform initialization, for fundamental analysis, and realistic scenarios with insulation losses and stratification, for practical applicability. This dual approach enables a robust evaluation of the performance of three-serpentine thermocline TES systems under different operating modes.

# 3.6 Numerical Setup and Discretization

A reliable CFD analysis requires not only an accurate physical model but also careful attention to the numerical setup. The discretization of the computational domain, selection of solver settings, and verification of independence from mesh size and time step are all crucial for ensuring that results are physically meaningful and not artifacts of the numerical method.

### 3.6.1 Mesh Generation

The computational domain is discretized using an unstructured mesh with refinement in regions of high gradients. Particular attention is given to:

• Serpentine walls: prism layers are added around the coil boundaries to resolve steep temperature and velocity gradients in the near-wall region.

• Bulk domain: a coarser mesh is used where gradients are mild, reducing overall computational cost.

The mesh is generated such that the aspect ratio of cells remains within recommended limits to maintain numerical stability. A compromise between accuracy and computational feasibility is achieved by keeping the total number of elements within a range manageable by available computing resources.

Surface Remesher, Polyhedral Mesher, Automatic Surface Repair and Prism Layer Mesher are selected in Mesher settings.

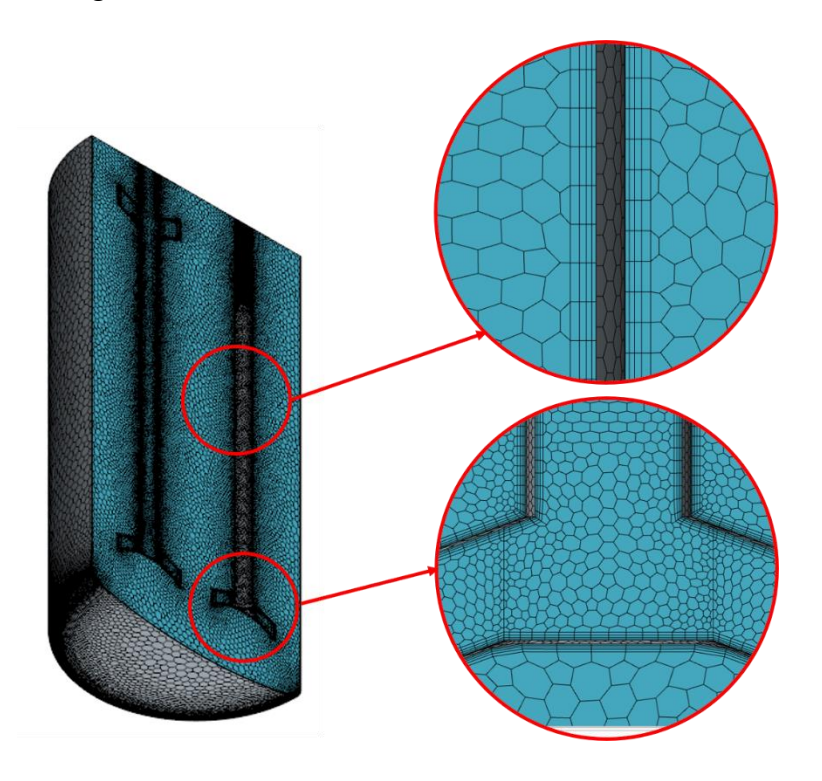


Figure 6 - Mesh generation and Prism layers

# 3.6.2 Grid Independence Study

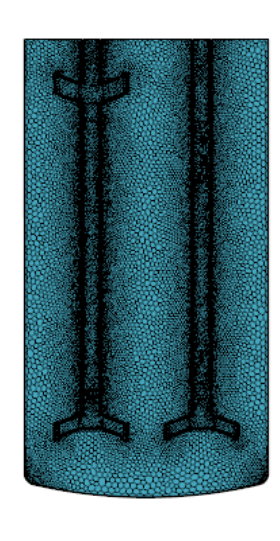
To ensure that results are not sensitive to mesh resolution, a grid independence study is performed. Simulations are run on progressively finer meshes, and the temperature at monitoring point and mass flow rate in the CSP channel as the key output parameters are compared. Once the variation between two successive refinements falls below an acceptable threshold, the coarser of the two meshes is selected for the final simulations.



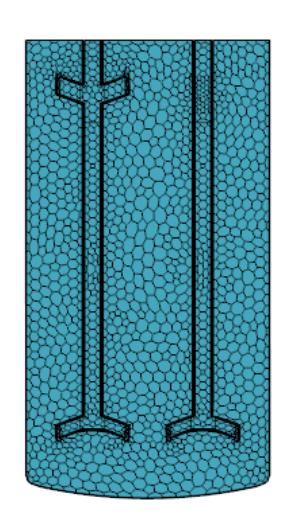




Cells number 998,384



Cells number 389,380

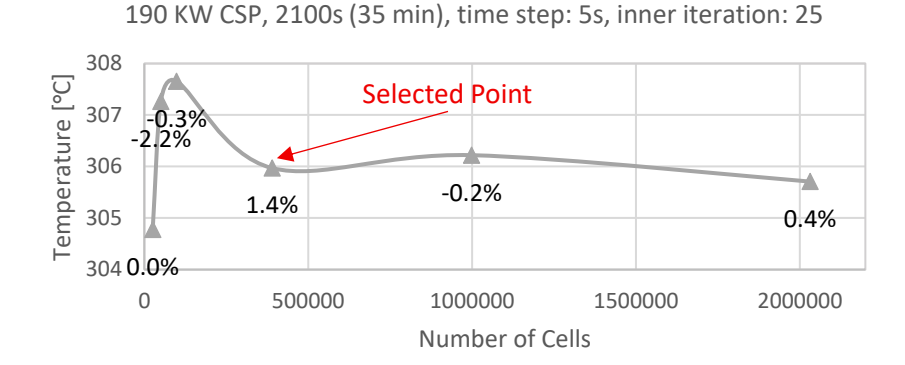


Cells number 25,424

Figure 7 - Mesh quality

Table 1 - Grid Independence Study

Base Size [m]	0.006	0.01	0.05	0.15	0.25	0.45	
Number of Cells	2031089	998384	389380	98172	50204	25424	
Growth %	103%	156%	297%	96%	97%	0%	
T[°C] @ y=2.30 [m]	305.708	306.221	305.971	307.657	307.263	304.778	
Growth %	0.4%	0.2%	1.4%	0.3%	2.2%	0.0%	
Mass Flow Rate [Kg/s]	2.057	2.059	2.071	2.0218	2.008	1.9763	
Growth %	0%	1%	2%	1%	2%	0%	
Run-Time [min]	4380	1800	900	180	120	50	
Growth %	143%	100%	400%	50%	140%	0%	



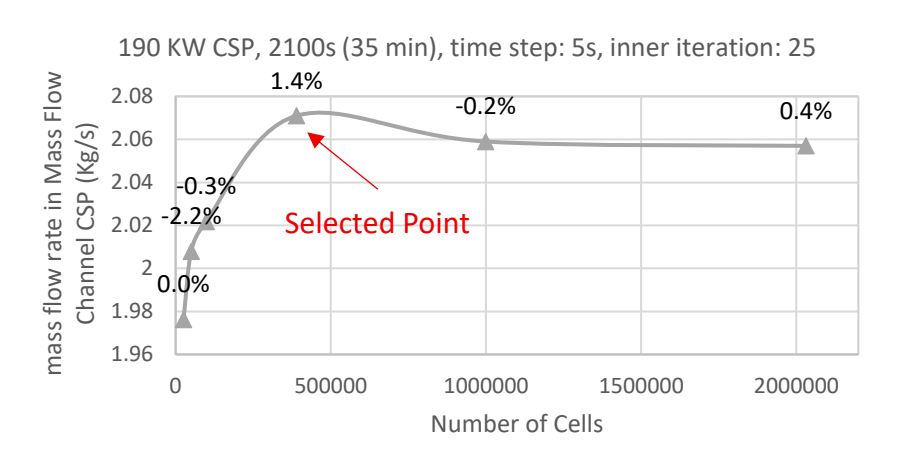


Figure 8 - Grid Independence Study graph: Temperature vs Number of cell and Mass flow rate vs Number of cell

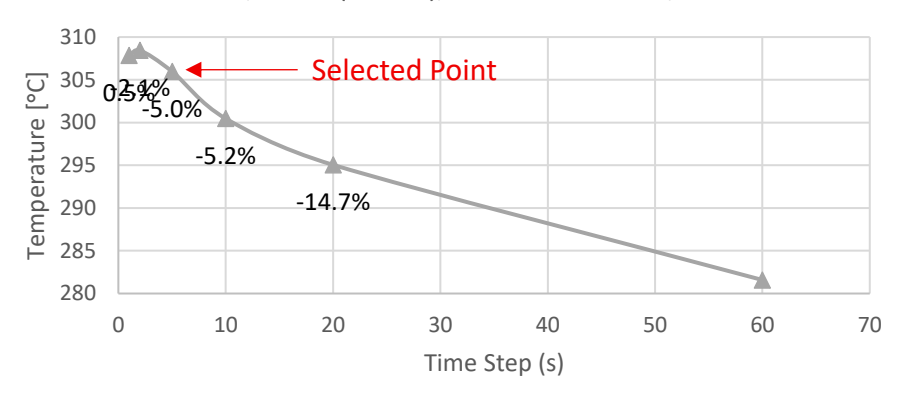
# 3.6.3 Time Step Sensitivity

The simulations are conducted in transient mode, requiring discretization of time. An implicit time integration scheme is chosen for stability, especially under buoyancy-driven flow conditions. A time-step sensitivity study is carried out by running cases with progressively smaller time steps. The selected time step provides a balance between temporal resolution and computational cost, with relative differences in monitored parameters maintained below a set tolerance.

Table 2 - Time Step Sensitivity

Number of Cells	4.00E+05	4.00E+05	4.00E+05	4.00E+05	4.00E+05	4.00E+05	
time step [s]	1	2	5	10	20	60	
Growth %	50%	60%	50%	50%	67%	0%	
T[°C] @ y=2.30 [m]	307.835	308.442	305.971	300.468	295.051	281.581	
Growth %	0.5%	2.1%	5.0%	5.2%	14.7%	0.0%	
Mass Flow Rate [Kg/s]	2.066	2.067	2.071	2.054	2.019	2.021	
Growth %	0%	0%	1%	2%	0%	0%	
Run-Time [min]	3600	1800	900	360	180	60	
Growth %	100%	100%	150%	100%	200%	0%	

190 KW CSP, 2100s (35 min), inner Iteration: 25, cells: 4e5



190 KW CSP, 2100s (35 min), inner Iteration: 25, cells: 4e5

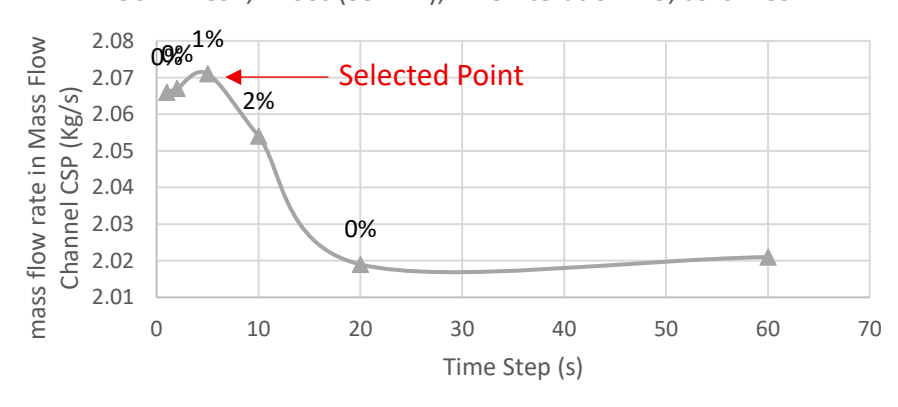


Figure 9 - Time Step Sensitivity graph: Temperature vs Time Step and Mass flow rate vs Time Step

# 3.6.4 Inner Iteration Sensitivity

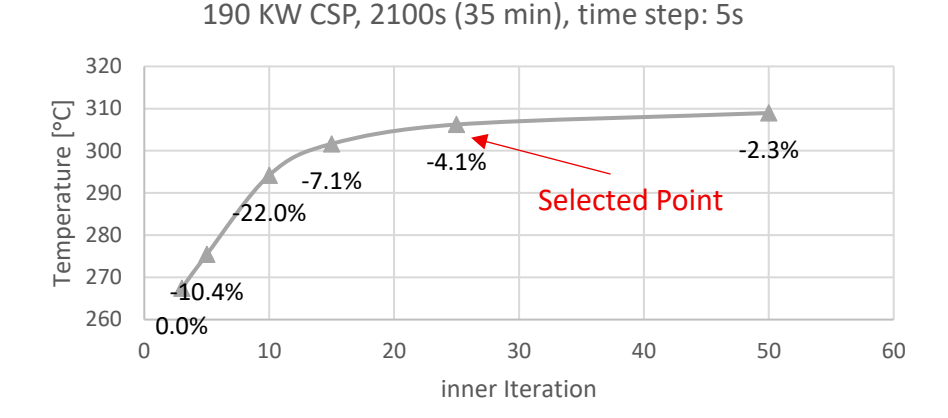
In transient CFD simulations, especially those involving strong temperature gradients and buoyancy-driven flows, the number of inner iterations per time step plays a crucial role in ensuring convergence of the coupled equations. If too few iterations are used, the residuals may not fall sufficiently at each time step, leading to numerical lag in the temperature and velocity fields. Conversely, excessive iterations increase computational time without significant improvement in accuracy.

To identify an optimal balance between accuracy and efficiency, an inner iteration sensitivity analysis was conducted. The number of inner iterations per time step was varied while monitoring the evolution of key output quantities such as temperature at monitoring point and mass flow rate in the CSP channel.

This inner iteration sensitivity verification confirms that the numerical solution is independent of solver iteration count, reinforcing the reliability of the transient laminar results for charging conditions.

Table 3 - Inner Iteration Sensitivity

Number of Cells	1.00E+06	1.00E+06	1.00E+06	1.00E+06	1.00E+06	1.00E+06	
inner Iteration	50	25	15	10	5	3	
Growth %	100%	67%	50%	100%	67%	0%	
T[°C] @ y=2.30 [m]	308.951	306.221	301.646	294.209	275.434	267.419	
Growth %	2.3%	4.1%	7.1%	22.0%	10.4%	0.0%	
Mass Flow Rate [Kg/s]	2.052	2.059	2.074	2.044	1.822	1.806	
Growth %	0%	1%	1%	12%	1%	0%	
Run-Time [min]	3600	1800	1080	660	360	210 0%	
Growth %	100%	67%	64%	83%	71%		



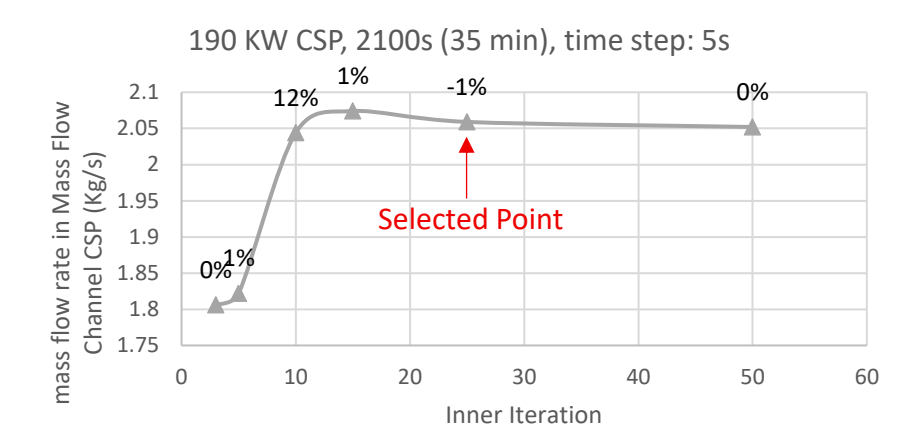


Figure 10 - Inner Iteration Sensitivity graph: Temperature vs Inner Iteration and Mass flow rate vs Inner Iteration

# 3.6.5 Solver Settings and Implemented Physical and Numerical Models

The simulation was performed using a pressure-based finite volume solver in transient mode. The following physical and numerical models were activated to accurately represent the laminar buoyancy-driven flow inside the thermocline tank while ensuring numerical stability:

- Three-dimensional, implicit unsteady formulation: the flow and temperature fields are solved as time-dependent 3D problems using an implicit time-stepping scheme to ensure numerical stability at larger time steps.
- Gravity and Boussinesq model: buoyancy forces are included through the Boussinesq approximation, where density variations are considered only in the gravity term.

- Constant density model: apart from the buoyancy term, the molten salt density is treated as constant to simplify pressure-velocity coupling.
- Laminar flow model: no turbulence model is used. Reynolds numbers remain within the laminar regime for all cases.
- Segregated solver for flow and temperature: momentum, pressure, and energy equations are solved sequentially to reduce computational cost.
- Solution interpolation and gradient reconstruction: second-order spatial discretization schemes are employed to minimize numerical diffusion, ensuring accurate resolution of the thermocline front.
- Cell quality remediation: activated to stabilize convergence in mesh regions with high aspect ratios, especially near the porous regions and thermocline interface.
- Liquid phase model: molten salt is treated as a single-phase liquid, with temperaturedependent viscosity and thermal properties.

These model selections ensure a stable and accurate simulation of natural and forced convection processes while maintaining computational efficiency for long transient runs.

### 3.7 Simulation Scenarios

The numerical study was designed to evaluate the thermal behavior of the thermocline TES system under different charging conditions and geometric configurations. Two groups of simulations were performed:

- 1. The first group focuses on different charging compositions from CSP and PV sources, analyzing how inlet power distribution affects the evolution of the thermocline and the time required to reach a specified outlet temperature.
- 2. The second group investigates the effect of orifices inside the PV/CSP channels, assessing how variations in their geometry and number influence stratification quality.

# 3.7.1 Scenarios Based on Inlet Power Composition

Four charging cases were simulated to represent typical and hybrid operation conditions of solar energy plants:

- 1. CSP-only case: charging power supplied entirely by the concentrated solar power source (CSP: 190 kW, PV: 0 kW).
- 2. PV-only case: charging power supplied entirely by the photovoltaic source (CSP: 0 kW, PV: 190 kW).
- 3. Balanced CSP/PV case: equal charging contribution from both sources (CSP: 95 kW, PV: 95 kW).
- 4. Combined high-power case: simultaneous maximum input from both sources (CSP: 190 kW, PV: 190 kW).

For each scenario, the simulation tracks the temporal evolution of the thermocline and determines the time required for the outlet temperature to reach 300 °C. This allows direct comparison of thermal response and storage performance under different hybrid input conditions. The thermocline structure is also monitored over time to assess its stability and sharpness during the charging process.

### 3.7.2 Effect of Orifices on the PV/CSP Channels

To improve thermal stratification, a second group of simulations examines the inclusion of orifices within the PV/CSP Channels. Three geometric parameters are investigated:

- Position of orifices
- Radius of orifices
- Number of orifices

The objective of these tests is to identify the combination of orifice parameters that yields the most uniform flow field and the most stable thermocline profile during charging and discharging cycles.

# 3.7.3 Evaluation Criteria

Across all simulations, performance is compared using the following indicators:

- Time to reach target outlet temperature (300 °C),
- Thermocline thickness and evolution over time,
- Overall improvement in stratification quality relative to the reference case without orifices.

# Chapter 4 Results & Discussion

### 4.1 Overview of the Simulation Process

The transient CFD simulations were performed using the setup described in Chapter 3. The selected computational parameters were as follows:

• Inner iterations per time step: 25

• Time step size: 5 s

• Base mesh size: 0.05 m, approximately 4×10<sup>5</sup> cells

Each simulation was carried out until the temperature at the upper monitoring point, Y = 2.30 m, reached 300 °C, corresponding to the desired thermal charge level. The analysis focused on the temperature and velocity contours, temperature—time histories, and vertical temperature distributions to assess thermocline development, sharpness, and stability.

Two main sets of cases were considered:

- 1. Thermocline evolution under different CSP/PV inlet power combinations
- 2. The effect of orifice geometry on stratification including position, radius and number.

### 4.2 Effect of Inlet Power Composition on Thermocline Formation

Four power input combinations were simulated to represent typical operating modes of hybrid CSP-PV charging:

- CSP-only (190 kW)
- PV-only (190 kW)
- Balanced CSP/PV (95 kW each)
- Combined high-power CSP/PV (190 kW each)

### **4.2.1 Temperature Evolution**

Temperature contours clearly illustrate that the thermocline develops progressively from the bottom of the tank, where heat is injected, and rises upward as charging proceeds. The time

required for the upper region (Y = 2.30 m) to reach 300 °C varies considerably across the different charging scenarios:

Table 4 - Different Charging Scenarios

Case	CCD Down [lvW]	DV Dower [l/W]	Time to reach 300 °C		
Case	CSP Power [kW]	PV Power [kW]	[min]		
CSP only	190	0	32		
PV only	0	190	34		
CSP-PV balanced	95	95	38		
CSP-PV combined	190	190	17		

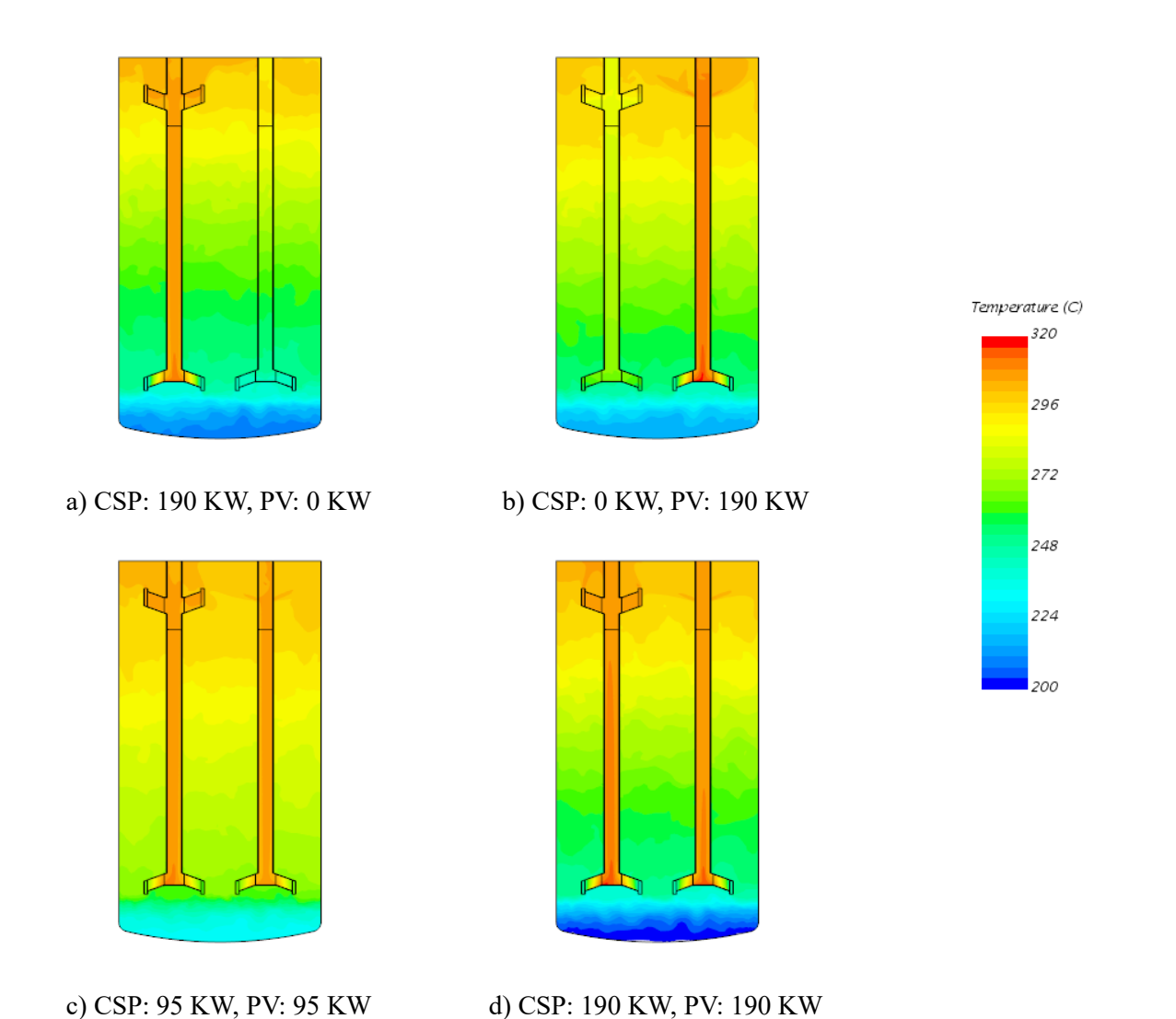


Figure 11 - Temperature contour for different charging scenarios

The results show that a higher total power input noticeably accelerates the charging process. When both energy sources operate at full capacity, the molten salt inside the tank warms up much faster, and the upper region reaches higher temperatures in a shorter time. The combined effect of the two heat sources creates a stronger heating intensity, causing the hot layer at the top of the tank to expand more rapidly. In this case, the temperature of 300°C is achieved in about half the time required for single-source operation, demonstrating the significant influence of total power on charging performance.

In contrast, when the total heat input is reduced, such as in the balanced CSP-PV configuration, the overall heating rate slows down. The temperature rise becomes more gradual, and the formation of the hot layer at the top of the tank takes longer. The difference in total power clearly affects how quickly the system can store heat and reach the desired temperature level.

### 4.2.2 Temperature-Time Behavior

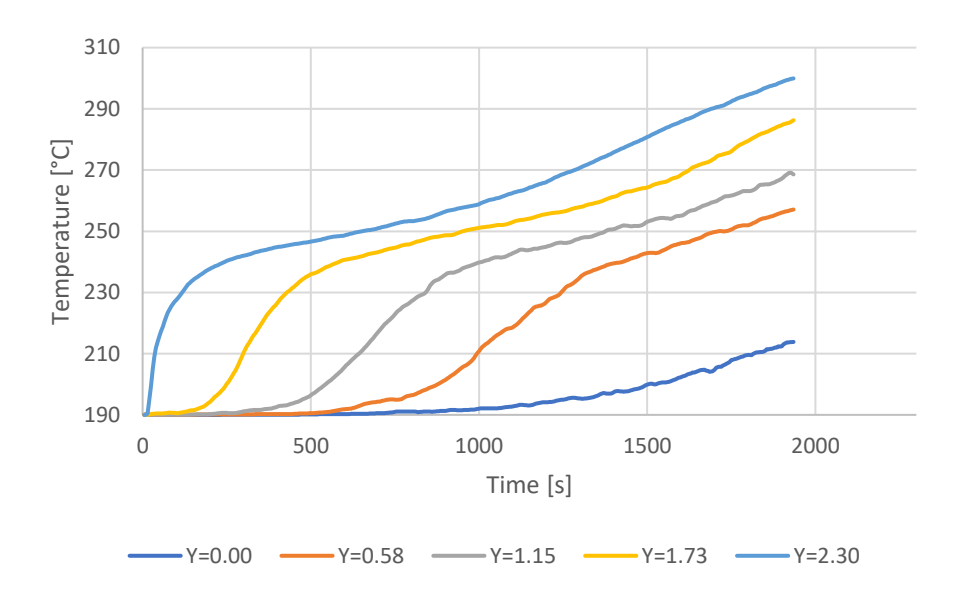
The temperature—time curves recorded at different vertical positions (Y = 0.00, 0.58, 1.15, 1.73, and 2.30 m) clearly show that the heating process begins in the upper region of the tank and then gradually extends downward as charging continues. At the start of the simulation, the temperature near the top increases sharply, forming a distinct hot layer that progressively grows thicker with time. The lower sections, being farther from the region of strongest heating, show a slower and more gradual temperature rise.

As the process continues, the difference between the upper and lower temperature readings becomes more evident, illustrating the formation of a well-defined thermocline. The temperature at intermediate heights rises after a certain delay, indicating the downward movement of the thermal front. The slopes of the curves at these positions confirm that the heating process in the molten salt occurs progressively from the top toward the bottom of the tank.

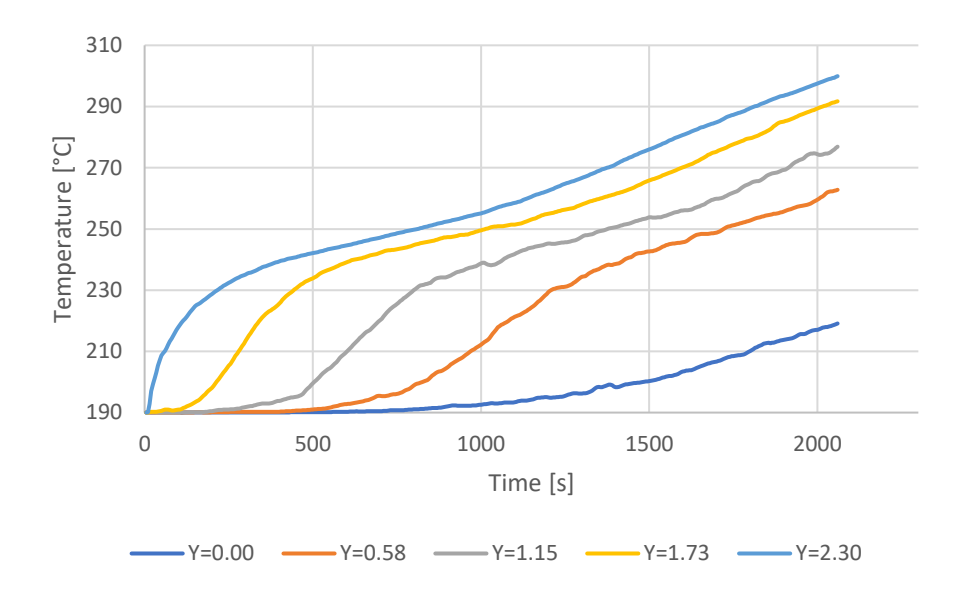
Over time, the temperature growth rate in the upper region starts to decrease as the hot layer stabilizes and the heat distribution within the molten salt becomes more uniform. The gradual flattening of the temperature curves in the upper levels reflects the approach to thermal equilibrium in that part of the tank, while the lower regions continue to warm up slowly. This behavior demonstrates that the heat stored at the top of the tank diffuses downward through natural

convection and conduction, maintaining a smooth and continuous transition between hot and cold zones.

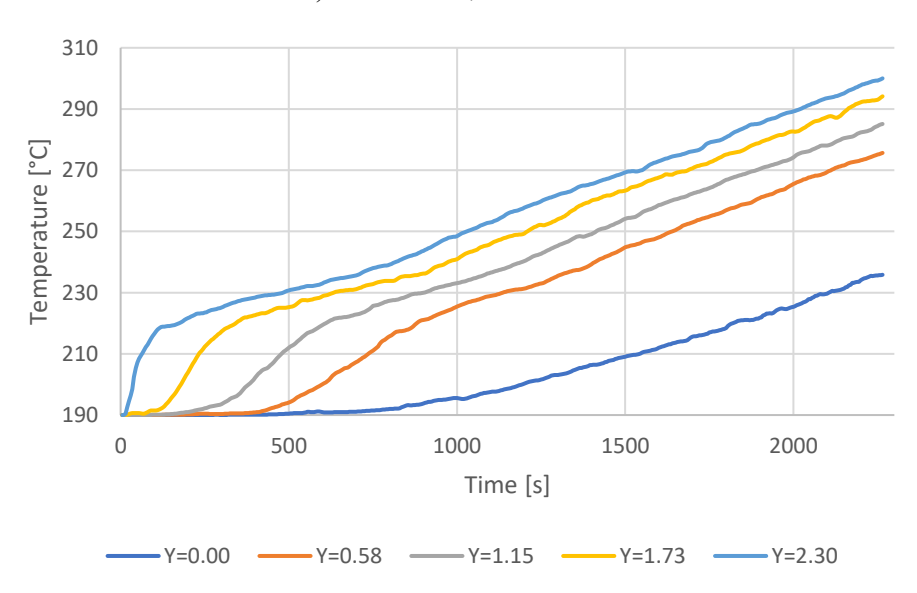
Overall, the temperature-time behavior confirms that the charging process develops from the top downward, with the hot layer expanding steadily as energy is supplied. The rate of this progression depends strongly on the total power input: higher power leads to a faster expansion of the hot region and shorter charging times, whereas lower power results in a slower and more gradual thermal response. However, in the balanced configuration, where both sources provide equal but moderate power, the temperature at the bottom of the tank is noticeably higher than in the other configurations at the moment when the top reaches 300°C. This indicates that the thermal front becomes more diffused and the temperature gradient along the tank height is weaker. Such behavior reflects a loss of thermal stratification, which is undesirable for efficient energy storage, as it reduces the distinction between hot and cold zones and lowers the overall quality of the stored heat.



a) CSP: 190 KW, PV: 0 KW



b) CSP: 0 KW, PV: 190 KW



c) CSP: 95 KW, PV: 95 KW

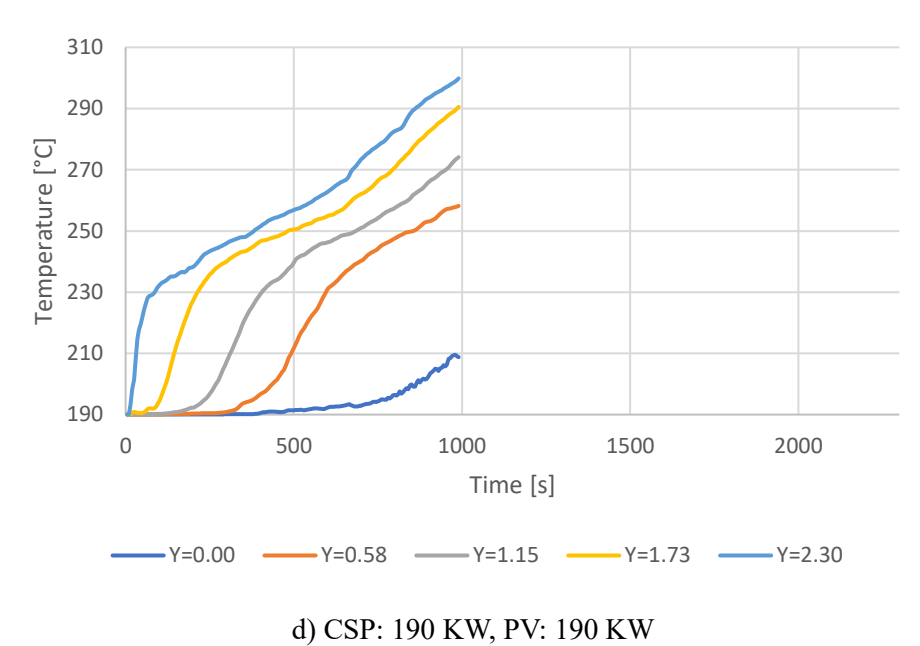


Figure 12 - Temperature vs Times for different charging scenarios

# 4.2.3 Velocity Field Analysis

The velocity contours provide further insight into the thermal behavior of the system under different power inputs. In all configurations, the velocity inside the main volume of the tank remains extremely low throughout the charging process, indicating that fluid motion is negligible in this region. The flow field shows only slight circulation near the top, but these motions are too weak to contribute significantly to heat transport. This confirms that within the tank, conduction is the dominant heat transfer mechanism, with temperature rising mainly through thermal diffusion from the hotter upper layers.

In contrast, noticeably higher velocities are observed inside the active channel region, where the heat source is applied. The movement of fluid in this area is much more pronounced, showing that convection is dominant inside the channel. The warmer fluid in this zone tends to move upward along the heated region, while cooler fluid from surrounding areas slowly replaces it. This localized circulation within the channel region enhances internal heat exchange and contributes to the formation of the hot layer in the upper part of the tank.

Comparing the different power input scenarios, it can be seen that higher total power results in slightly stronger velocity magnitudes inside the channel, consistent with the faster temperature rise

observed in previous sections. However, the overall flow intensity within the tank remains low for all cases, reinforcing that heat transfer in the bulk of the molten salt occurs mainly by conduction rather than convection.

This combined behavior, dominant convection within the heating channel and dominant conduction in the tank, explains the gradual, top-down temperature increase observed in the system. The hot region expands primarily due to heat diffusion from the upper layers rather than large-scale fluid motion, which aligns well with the laminar and low-velocity characteristics of the simulated flow field.

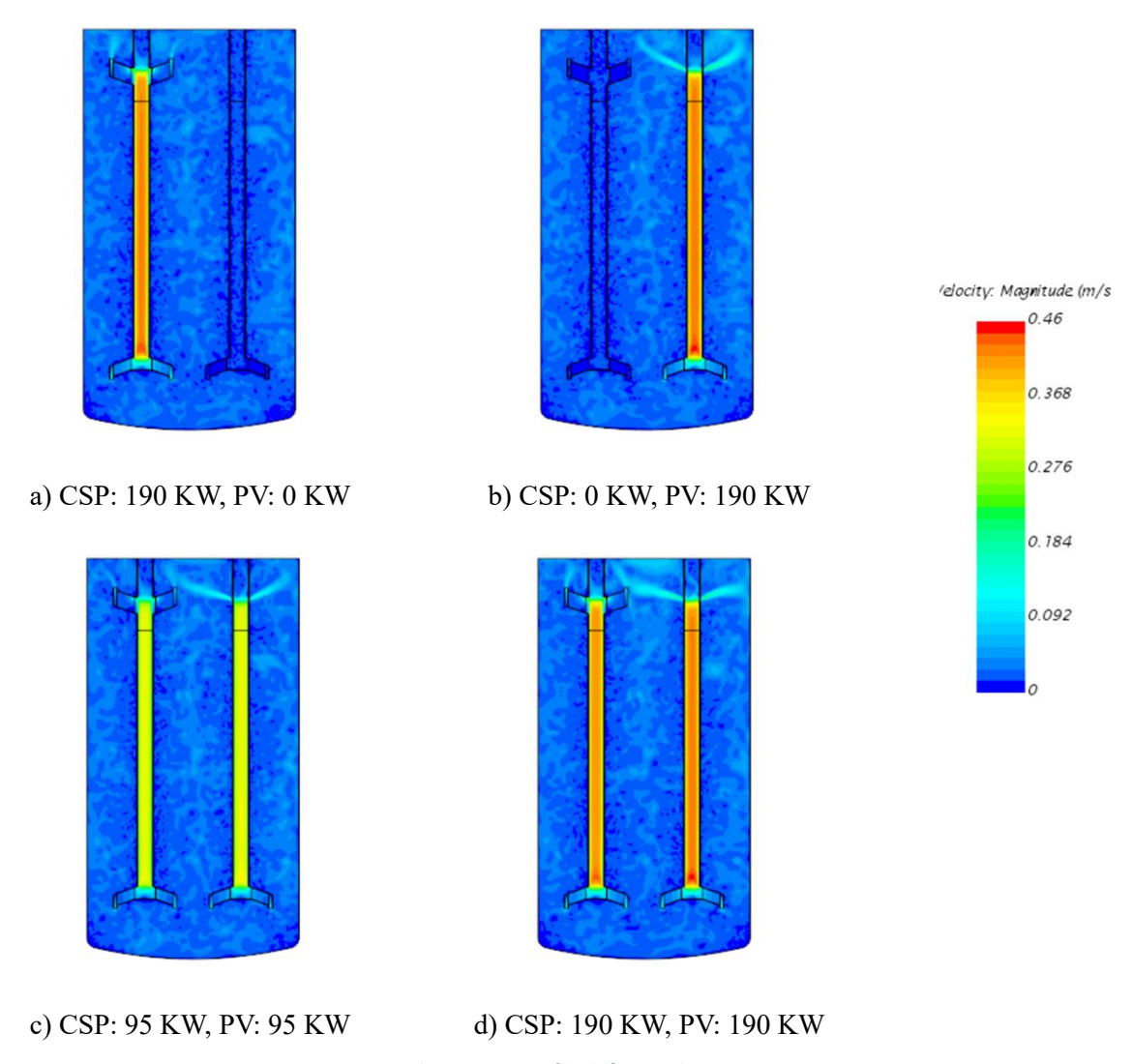


Figure 13 - Velocity contour for different charging scenarios

### 4.2.4 Vertical Temperature Distribution

The vertical temperature profiles provide a clear representation of the thermocline shape and its evolution under different charging conditions. The results show that, in all configurations, the temperature decreases gradually from the top toward the bottom of the tank, confirming that the tank warms from the upper region downward. The temperature gradient between the hot and cold layers is relatively smooth, and no sharp interface is formed between them. This indicates that the thermocline layer is relatively thick, meaning that the thermal stratification quality is not ideal in any of the studied cases.

Comparing the four power configurations, it is observed that the balanced CSP/PV case, 95 kW each, produces the thickest thermocline. The more moderate total heat input in this configuration results in a slower heating process and a weaker distinction between the hot and cold regions. The gradual temperature transition through the tank height indicates that the stored heat is more evenly distributed, but the lack of a distinct thermal boundary reduces stratification efficiency.

For the other three cases, CSP-only, PV-only, and combined high-power CSP/PV, the thermocline profiles are very similar, showing comparable temperature gradients along the tank height. Among them, the double high-power configuration shows a slightly sharper thermal transition near the upper part of the tank. The higher energy input in this case enhances local heating, leading to a marginal improvement in thermocline definition. However, this effect remains limited, and even in the best case, the thermocline cannot be considered well-defined.

Overall, the vertical temperature analysis demonstrates that none of the current configurations produce a strong and stable thermocline. The transition region between hot and cold layers remains wide, resulting in a significant loss of thermal stratification. Therefore, to improve stratification and enhance thermal performance, geometric modifications such as the implementation of orifices inside the charging channel are proposed and investigated in the following section.

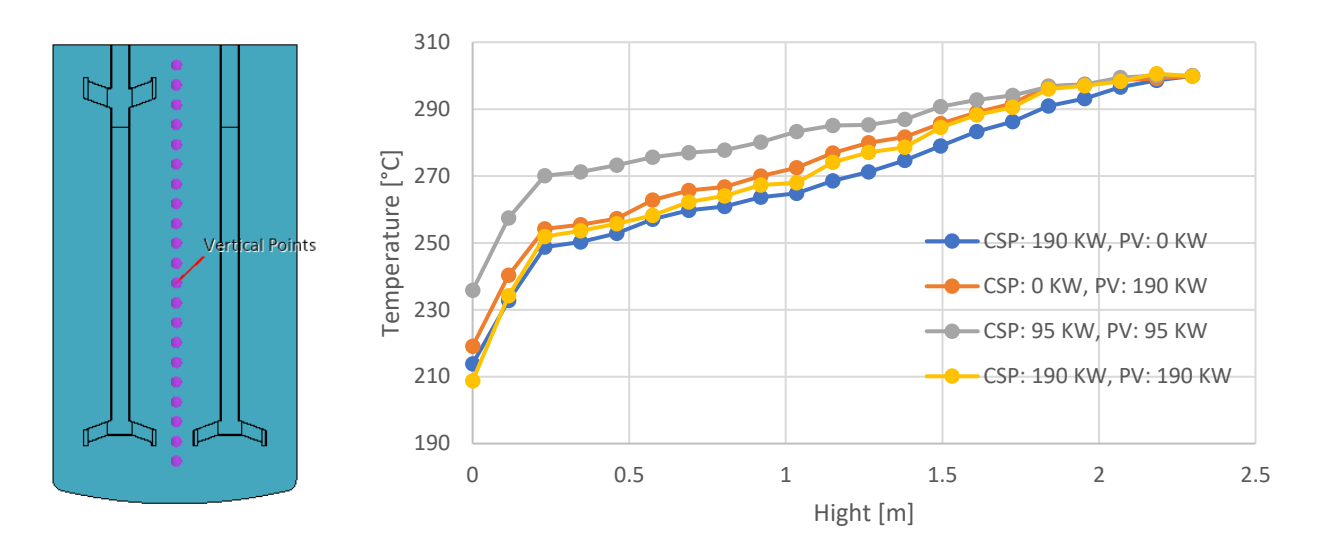
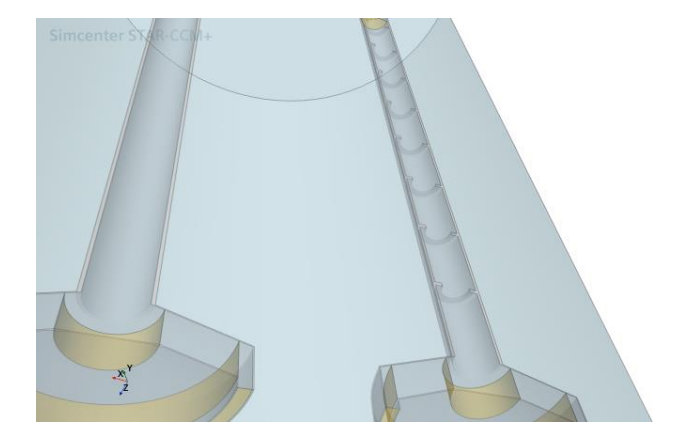


Figure 14 - Thermocline formation for different charging scenarios

### 4.3 Effect of Orifices on Thermal Stratification

The results obtained from the previous cases showed that the thermocline formed inside the tank was relatively thick and not well defined, indicating that the stratification quality was unsatisfactory. To improve the temperature distribution and obtain a more stable thermocline, additional simulations were performed by implementing orifices arranged in series along the channels. These orifices influence the movement of the heated molten salt inside the channels before it exits into the upper part of the tank.



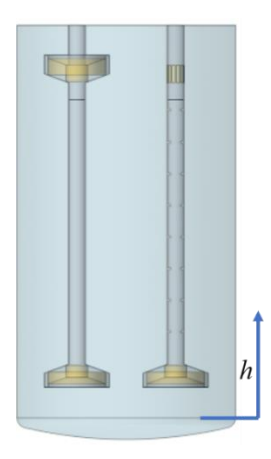


Figure 15 - The geometry of orifices

Several configurations were examined by varying the position, radius, and number of orifices, to study how these parameters affect the flow behavior inside the channels and the resulting temperature distribution in the molten salt. The following sections present the outcomes of these simulations and evaluate the influence of each parameter on the thermocline formation.

Table 5 – List of simulated cases to analyze the effects of position, radius and number of orifices

No.	of	1	2	3	4	5	6	7	8	9	10	11	12	13	14	15	16	17
Case		1	2	3	7	J	U	,	O	,	10	11	12	13	17	13	10	17
No.	of	2	2	2	2	2	2	2	2	2	3	4	6	8	6	8	6	8
Orific	ces	2	2	2	2	2	2	2	2	2	3	7	U	o	O	o	U	O
Radiu	1S	30	20	30	30	27.5	25	22.5	17.5	35	30	30	27.5	27.5	26.25	26.25	30	30
[mm]		30	20	30	30	21.3	23	22.3	17.3	33	30	30	21.3	21.3	20.23	20.23	30	30
	h1	0.7	0.7	1	0.5	0.7	0.7	0.7	0.7	0.7	0.6	0.6	0.5	0.5	0.5	0.5	0.5	0.5
	h2	1.8	1.8	1.5	1.5	1.8	1.8	1.8	1.8	1.8	1.2	1	0.76	0.685	0.76	0.685	0.76	0.685
	h3										1.8	1.4	1.02	0.87	1.02	0.87	1.02	0.87
ı] mc	h4											1.8	1.28	1.055	1.28	1.055	1.28	1.055
botta	h5												1.54	1.24	1.54	1.24	1.54	1.24
Position from bottom [m]	h6												1.8	1.425	1.8	1.425	1.8	1.425
	h7													1.61		1.61		1.61
Posi	h8													1.8		1.8		1.8

Based on the results provided in Fig. 16, the presence of orifices arranged in series along the channels changes the flow behavior of the molten salt and the way heat is transferred to the bulk fluid in the tank. As the molten salt passes through the orifices, the reduced cross-section modifies the velocity distribution inside the channels, accelerating the flow at the centerline and slowing it down near the walls. This adjustment of the flow pattern allows the fluid to reach a higher temperature by the time it exits the channels. Consequently, the molten salt entering the upper part of the tank is hotter and moves more slowly compared with the case without orifices.

This difference in outlet conditions has a strong effect on the charging process. After 900 seconds, the tank equipped with orifices reaches approximately 290 °C, while the configuration without orifices achieves only about 250 °C. The lower outlet velocity associated with the orifices results in a gentler release of the hot fluid, limiting mixing near the top region of the tank and producing

a clearer separation between hot and cold zones. The combined effect of the higher outlet temperature and reduced flow intensity leads to a faster charging process and a more distinct thermocline. Overall, the implementation of orifices inside the channels enhances both the heating efficiency and the stability of thermal stratification within the storage system.

The results of these simulations are presented and discussed in the following section.

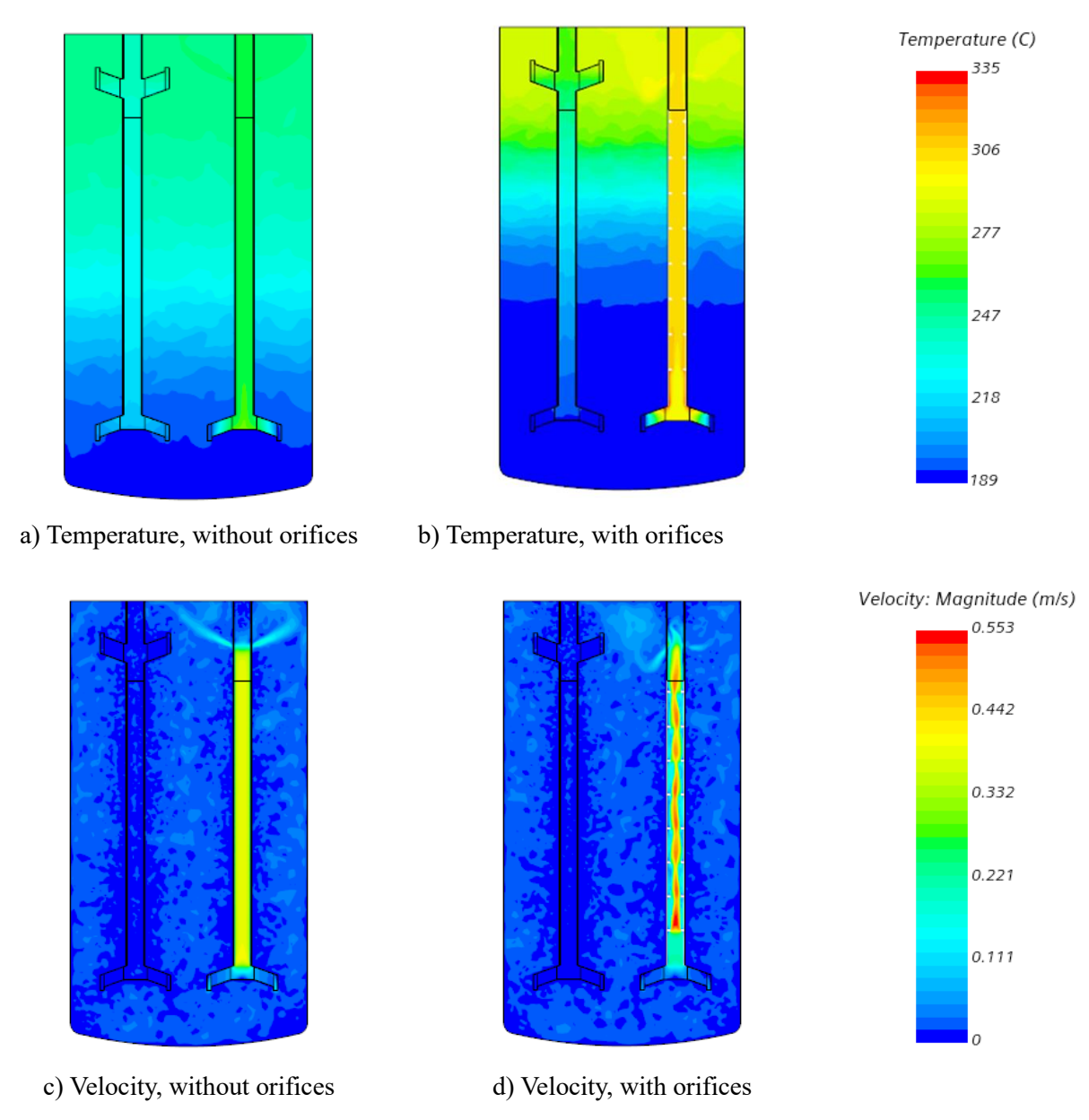


Figure 16 - Numerical simulation contours after 900s of charging in presence of orifices

### 4.3.1 Influence of Orifice Position

To study the effect of orifice position, several cases were simulated with the same number and size of orifices but placed at different heights along the channels. The results show that the thermocline profiles are nearly identical for all tested positions. In each case, the temperature gradient improves compared with the configuration without orifices, but the differences among the various orifice placements are negligible. This indicates that the vertical position of the orifices has a minimal effect on the overall temperature distribution or stratification pattern inside the tank. In all configurations, the presence of orifices enhances the thermal layering to a similar extent, suggesting that the precise placement of the orifices along the channels is not a critical factor for improving thermocline performance.

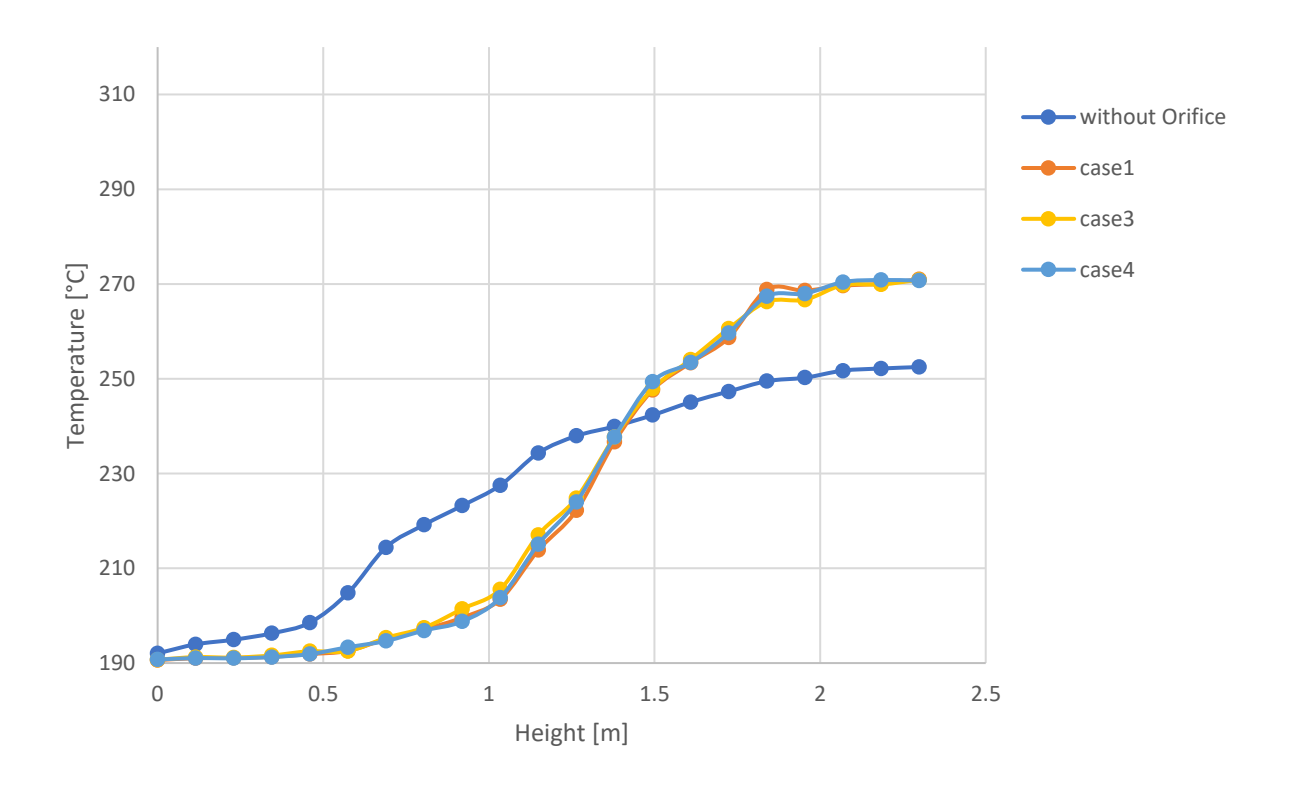


Figure 17 - The effect of orifices position

### 4.3.2 Influence of Orifice Radius

The impact of orifice radius was examined by comparing channels with different orifice sizes while keeping the number and position of orifices constant. The results show that smaller orifices lead to a more stable and sharper thermocline, while larger ones produce a thicker temperature transition. The reduced diameter of the orifices causes a lower velocity at the channel outlet, allowing the heated molten salt to enter the upper region of the tank more smoothly. This gentler discharge limits the mixing between hot and cold layers and helps maintain a better temperature gradient. As a result, the tank with smaller orifices warms up more effectively and reaches higher temperatures in a shorter time. These results confirm that reducing the orifice radius improves both the charging rate and the thermal stratification of the system.

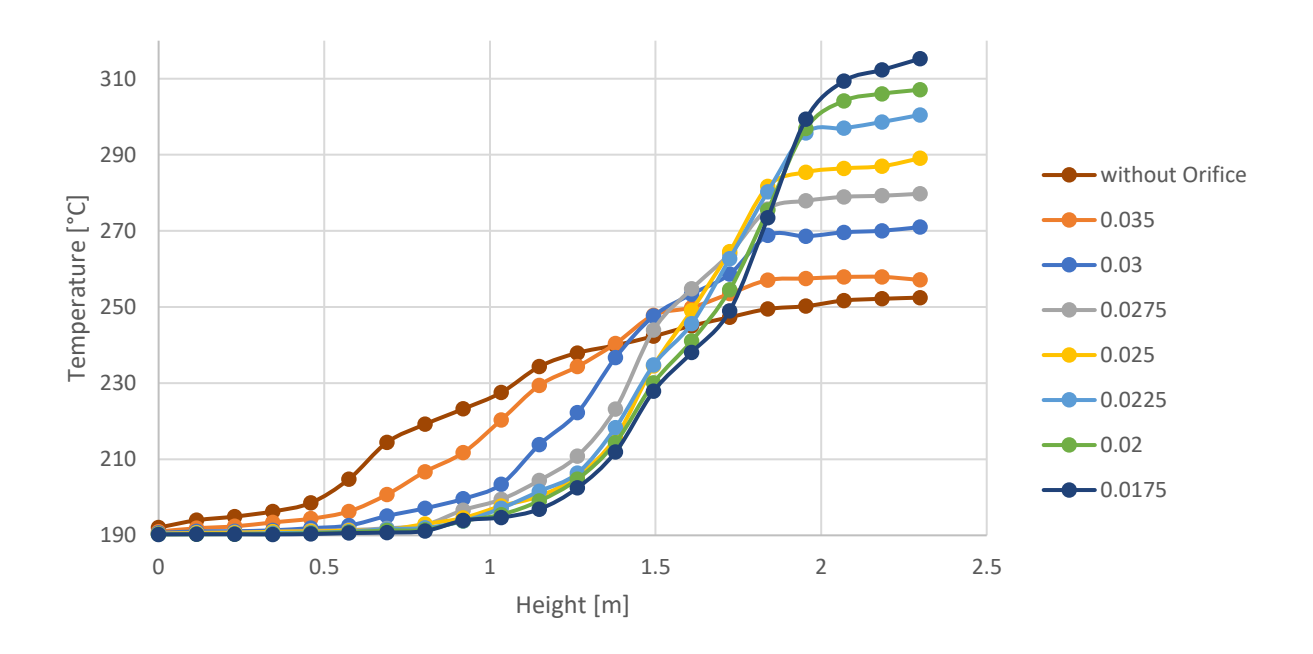


Figure 18 - The Effect of Orifices Radius

### 4.3.3 Influence of Number of Orifices

The influence of the number of orifices was evaluated by simulating channels with different counts of orifices arranged in series. The results demonstrate that increasing the number of orifices improves the thermocline, leading to a thinner and more uniform temperature transition. A greater number of orifices provides smoother heat release along the channels, reducing flow velocity at the outlet and minimizing temperature mixing near the upper region of the tank. At the same time, the presence of multiple orifices introduces slightly higher flow resistance within the channels, which lowers the overall flow intensity but enhances the stability of stratification. Consequently, configurations with more orifices produce higher outlet temperatures, a clearer thermocline, and a faster rise in the tank's average temperature.

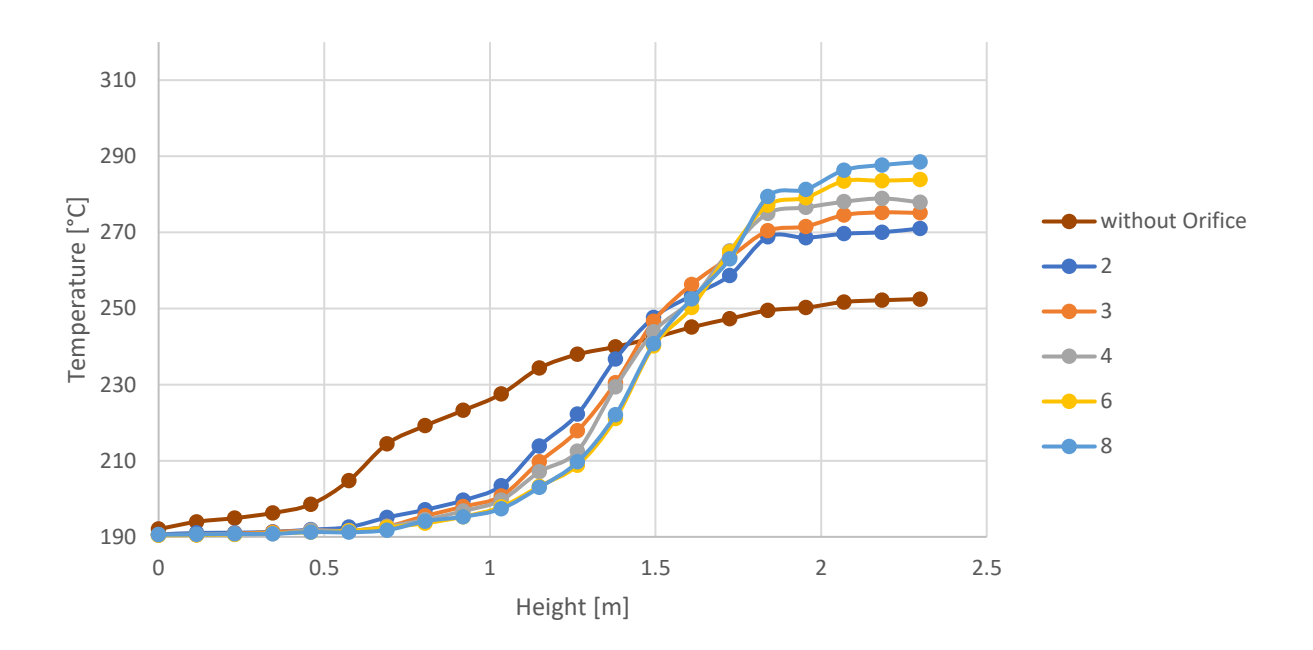


Figure 19 - The Effect of Number of Orifices

### 4.3.4 Comparison with Reference Case

The influence of the number of orifices was examined by comparing cases with different counts of openings along the channels. The results show that increasing the number of orifices produces a thinner and better-defined thermocline, improving the overall temperature stratification inside the tank. When more orifices are present, the heated molten salt is released in smaller and more distributed streams, which lowers the local flow intensity and minimizes mixing near the upper part of the tank. This results in a smoother and more stable temperature gradient between the hot and cold regions.

At the same time, the presence of multiple orifices introduces greater flow resistance within the channels, leading to a slight pressure drop along their length. This reduction in flow strength contributes to a gentler heat release into the surrounding molten salt, supporting the maintenance of stratification. Although the flow resistance increases, the overall effect of adding more orifices is positive, as the improved temperature layering enhances the thermal performance and stability of the storage system.

#### 4.4 Discussion

The simulation results clearly show how the configuration of the heating channels and the use of orifices affect the thermal behavior of the storage system. In the first part of the study, different CSP–PV power combinations were analyzed. It was observed that increasing the total input power shortens the charging time, as the molten salt reaches higher temperatures more rapidly. However, despite the difference in heating rate, the thermocline remained relatively thick in all cases, and the balanced CSP–PV configuration exhibited the weakest stratification. These results indicated that the baseline design was unable to produce a sharp thermal separation between the hot and cold regions, motivating the introduction of orifices in the following simulations.

The second part of the analysis focused on the effect of orifices arranged in series along the channels. Their presence significantly improved the temperature distribution inside the tank. The outlet velocity decreased, while the outlet temperature increased, producing a gentler and more effective release of heat into the upper region. This behavior resulted in a faster overall charging process and a better-defined thermocline. After 900 seconds, the system with orifices reached

approximately 290 °C, compared with 250 °C for the configuration without orifices. Among the tested parameters, orifice position showed negligible influence, whereas smaller radius and a higher number of orifices provided the most favorable results.

All in all, the implementation of orifices along the heating channels enhances the charging efficiency and improves thermal stratification by modifying the flow pattern and reducing mixing in the upper part of the tank. Although all cases with orifices performed better than the reference configuration, the best thermal behavior was obtained with smaller and more numerous orifices, confirming their effectiveness as a simple and efficient design improvement for thermocline thermal energy storage systems.

# Chapter 5 Conclusion

### 5.1 Summary of the Work

The objective of this thesis was to investigate the thermal behavior of a thermocline thermal energy storage (TES) system equipped with three internal channels, focusing on the effect of different charging conditions and the introduction of orifices along the channels. The study was carried out through a detailed computational fluid dynamics (CFD) analysis based on laminar, natural-convection heat transfer using molten salt as the storage medium.

The first part of the work examined the influence of different charging power compositions from concentrated solar power (CSP) and photovoltaic (PV) sources on the thermocline formation and the temperature distribution inside the storage tank. Four scenarios were simulated, including CSP-only, PV-only, balanced CSP-PV, and simultaneous high-power CSP+PV operation. The analysis provided insight into how the total power input affects the rate of charging, the temperature evolution, and the quality of thermal stratification.

The second part of the study introduced orifices arranged in series along the channels as a passive design modification to improve stratification. Several configurations were analyzed by varying the orifice position, radius, and number. This parametric study aimed to understand how the flow adjustments within the channels influence the temperature field in the molten salt and the overall performance of the thermal storage process.

# 5.2 Key Results and Findings

The simulations revealed clear trends in the thermal and flow behavior of the system. For the first set of analyses, the results showed that the total power input has a major effect on the charging rate of the tank. Higher total power accelerates the temperature rise and allows the target temperature at the top of the tank to be reached in a shorter time. In particular, the simultaneous high-power CSP+PV configuration reached 300 °C in about half the time of the single-source cases. In contrast, the balanced CSP-PV configuration exhibited a slower heating rate and weaker stratification. Despite these differences in charging speed, the thermocline structure remained relatively thick in all cases, indicating that the temperature transition between hot and cold regions was gradual and that the overall stratification quality was limited.

Because the thermocline in all baseline cases was not well defined, the next phase of the study introduced orifices to improve the temperature distribution. The presence of orifices inside the channels was found to significantly influence both the temperature field and the charging process. The molten salt flowing through the orifices experienced a redistribution of velocity, characterized by higher flow speeds near the channel centerline and lower speeds close to the walls. This adjustment resulted in a lower outlet velocity and a higher outlet temperature when the fluid entered the tank. Consequently, the tank equipped with orifices reached approximately 290 °C after 900 seconds, while the configuration without orifices reached only about 250 °C during the same period.

The comparison among different orifice geometries confirmed that the position of the orifices along the channels has a negligible impact on the thermocline profile, while the radius and number of orifices play a decisive role. Smaller orifices and a higher number of openings in series produced the best results, yielding a thinner and more stable thermocline. The smaller cross-sections reduced the outlet velocity, limited the extent of mixing at the top of the tank, and allowed a more uniform heat release. Increasing the number of orifices had a similar effect by spreading the heating more evenly along the channels, improving the layering of the molten salt. These configurations also exhibited a small pressure drop along the channels, but this was beneficial for the stratification since it further reduced turbulent disturbances and maintained a gentler temperature gradient.

Overall, the study demonstrated that the addition of orifices not only improved stratification but also accelerated the charging process, allowing the tank to reach higher temperatures in less time. The improved thermocline definition increases the efficiency of thermal energy storage and makes the system more effective for use in hybrid CSP–PV power plants, where stable and predictable temperature control is essential.

### 5.3 Recommendations and Future Work

Building on the results of this study, several directions are proposed for future development.

1. Development of a 3D CFD Reduced-Order Model:

Creating a reduced-order model based on the full 3D CFD results would enable faster parametric studies and real-time performance prediction of thermocline TES systems, supporting system optimization and control applications.

2. Investigation of Forced Convection Using an Impeller System:

Introducing and analyzing an internal impeller could provide insights into how controlled forced convection influences heat transfer enhancement, stratification stability, and overall charging efficiency.

3. Experimental Validation of the Numerical Model:

Building a scaled experimental setup would allow direct validation of the CFD results, verification of temperature distributions, and assessment of material performance under realistic operating conditions.

### References

- 1. Kuravi, S., Trahan, J., Goswami, D. Y., Rahman, M. M., & Stefanakos, E. K. (2013). Thermal energy storage technologies and systems for concentrating solar power plants. Progress in Energy and Combustion Science, 39(4), 285–319.
- 2. Zhao, J., Ma, W., & Yu, Q. (2015). *Numerical study of molten salt convection in a TES system with helical coil heat exchangers*. Renewable Energy, 77, 569–578.
- 3. Agelin-Chaab, M., & Ghorbani, N. (2017). *Numerical study of a hybrid PV/T and thermal energy storage system for building heating applications*. Applied Thermal Engineering, 127, 1232–1244.
- 4. Zanganeh, G., Khanna, R., Walser, C., Pedretti, A., Zavattoni, S., & Steinfeld, A. (2012). Experimental and numerical investigation of combined sensible–latent heat storage systems for solar power plants. Solar Energy, 86(10), 3084–3098.
- 5. Tamme, R., Bauer, T., Laing, D., & Steinmann, W. D. (2008). *Advanced thermal energy storage technology for parabolic trough*. Journal of Solar Energy Engineering, 130(4), 041006.
- Gil, A., Medrano, M., Martorell, I., Lázaro, A., Dolado, P., Zalba, B., & Cabeza, L. F. (2010). State of the art on high-temperature thermal energy storage for power generation.
   Part 1—Concepts, materials and modellization. Renewable and Sustainable Energy Reviews, 14(1), 31–55.
- 7. Zhao, J., Ma, W., & Yu, Q. (2015). Numerical study of molten salt convection in a TES system with helical coil heat exchangers. Renewable Energy, 77, 569–578.
- 8. Dutta, P., & Singh, R. (2010). *CFD analysis of thermal stratification in energy storage tanks*. Applied Thermal Engineering, 30(16), 2643–2654.
- 9. Micheli, D., & Rinaldi, F. (2019). *Numerical analysis of natural convection effects in molten salt thermocline thermal storage*. Applied Thermal Engineering, 162, 114255.

- Pan, C., Li, Y., Wang, Z., & Yang, Y. (2012). Numerical investigation of thermocline formation in molten salt storage tanks under natural convection. Applied Energy, 92, 298– 305.
- 11. Ho, C. K., & Iverson, B. D. (2014). Review of high-temperature central receiver designs for concentrating solar power. Renewable and Sustainable Energy Reviews, 29, 835–846.
- 12. Agelin-Chaab, M., & Ghorbani, N. (2017). Numerical study of a hybrid photovoltaic-thermal (PV/T) and thermal energy storage system for building heating applications. Applied Thermal Engineering, 127, 1232–1244.
- 13. Tian, Y., & Zhao, C. Y. (2013). A review of solar collectors and thermal energy storage in solar thermal applications. Applied Energy, 104, 538–553.
- 14. Saman, W., Bruno, F., & Halawa, E. (2014). *Thermal storage for solar power generation*. In Advances in Thermal Energy Storage Systems (pp. 227–248). Woodhead Publishing.
- 15. Hachicha, A. A., Rodríguez, I., & Oliva, A. (2014). *CFD modeling of a molten-salt thermocline storage tank during the charging process.* Applied Energy, 123, 47–57.
- 16. Micheli, D., & Rinaldi, F. (2019). *Numerical analysis of natural convection effects in molten-salt thermocline thermal storage*. Applied Thermal Engineering, 162, 114255.
- 17. Luzzi, L., Micheli, D., & Rinaldi, F. (2020). *Numerical investigation of active flow control in molten-salt thermocline tanks*. Solar Energy, 204, 243–255.
- 18. Flueckiger, S. M., Iverson, B. D., & Garimella, S. (2014). *Thermocline thermal energy storage for concentrating solar power plants: Analysis of heat-transfer media*. Journal of Solar Energy Engineering, 136(4), 041013.
- 19. Tian, Y., & Zhao, C. Y. (2013). A review of solar collectors and thermal energy storage in solar-thermal applications. Applied Energy, 104, 538–553.
- 20. Hachicha, A. A., Rodríguez, I., & Oliva, A. (2014). *CFD modeling of a molten-salt thermocline storage tank during the charging process*. Applied Energy, 123, 47–57.
- 21. Behar, O., Khellaf, A., & Mohammedi, K. (2013). *A review of studies on central receiver solar thermal power plants*. Renewable and Sustainable Energy Reviews, 23, 12–39.

- 22. Fernández, A. I., Barreneche, C., Belusko, M., Bruno, F., Cabeza, L. F., & Halawa, E. (2017). *Heat-transfer analysis in thermal energy storage: A review.* Renewable and Sustainable Energy Reviews, 68, 825–835.
- 23. Qiu, G., & Hayden, A. C. S. (2015). A comparative study of sensible and latent heat thermal storage for concentrating solar power. Renewable Energy, 83, 1023–1031.
- 24. Micheli, D., & Rinaldi, F. (2018). *Thermal-energy-storage integration in CSP-PV hybrid systems: Performance and economic assessment*. Energy Conversion and Management, 171, 1130–1142.
- 25. Ho, C. K., & Iverson, B. D. (2014). Review of high-temperature central receiver designs for concentrating solar power. Renewable and Sustainable Energy Reviews, 29, 835–846.
- 26. Xu, C., Li, X., Wang, Z., & He, Y. (2010). Experimental investigation on the thermal performance of molten-salt thermocline storage. *Applied Thermal Engineering*, 30(17-18), 2525–2532.
- 27. Bauer, T., Laing, D., & Tamme, R. (2012). Overview of PCMs for TES applications in CSP plants. *Solar Energy Materials and Solar Cells*, 99, 101–111.
- 28. Farid, M. M., Khudhair, A. M., Razack, S. A. K., & Al-Hallaj, S. (2004). A review on phase change energy storage: materials and applications. *Energy Conversion and Management*, 45(9–10), 1597–1615.
- 29. Bellan, S., Goswami, D. Y., & Stefanakos, E. (2017). Thermal analysis of molten salt heat exchangers for TES applications. *Energy Conversion and Management*, 149, 774–785.
- 30. Laing, D., Steinmann, W. D., Tamme, R., & Richter, C. (2006). Advanced storage concepts for parabolic trough power plants. *Solar Energy*, 80(10), 1283–1289.
- 31. Pan, C., Li, Y., Wang, Z., & Yang, Y. (2012). Numerical investigation of thermocline formation in molten salt storage tanks under natural convection. *Applied Energy*, 92, 298–305.
- 32. Micheli, D., & Rinaldi, F. (2019). Numerical analysis of natural convection effects in molten salt thermocline thermal storage. *Applied Thermal Engineering*, 162, 114255.

- 33. Bejan, A. (2013). Convection Heat Transfer. Wiley.
- 34. Dinker, A., Agarwal, M., & Agarwal, G. D. (2017). Numerical investigation of stratification in thermocline tanks with different heat exchanger placements. *Energy Procedia*, 109, 402–410.
- 35. Wu, Z., Yang, Y., & Wang, Z. (2015). Experimental study on the performance of a molten salt thermocline storage tank under natural convection. *Renewable Energy*, 83, 806–815.
- 36. Bradshaw, R. W., & Siegel, N. P. (2008). Molten nitrate salts for heat transfer and thermal energy storage in solar thermal systems. *Solar Energy*, 82(2), 125–133.
- 37. Bonk, A., Pauer, G., & Bauer, T. (2018). Characterization of thermophysical properties of molten salt mixtures for advanced TES systems. *Journal of Energy Storage*, 17, 221–229.
- 38. Singh, R., & Saini, R. P. (2017). A review on packed bed solar thermal energy storage using oils and molten salts. *Renewable and Sustainable Energy Reviews*, 73, 672–687.
- 39. Fazio, C., & Giancarli, L. (2015). Liquid metals for high-temperature TES: Thermophysical properties and technological challenges. *Journal of Nuclear Materials*, 465, 762–773.
- 40. Pacheco, J. E., Showalter, S. K., & Kolb, W. J. (2002). Development of a molten-salt thermocline thermal storage system. *Journal of Solar Energy Engineering*, 124(2), 153–159.
- 41. Micheli, D., & Rinaldi, F. (2019). Numerical analysis of natural convection effects in molten salt thermocline thermal storage. *Applied Thermal Engineering*, 162, 114255.
- 42. Wu, Z., Yang, Y., & Wang, Z. (2015). Experimental study on the performance of a molten salt thermocline storage tank under natural convection. *Renewable Energy*, 83, 806–815.
- 43. Dinker, A., Agarwal, M., & Agarwal, G. D. (2017). Numerical investigation of stratification in thermocline tanks with different heat exchanger placements. *Energy Procedia*, 109, 402–410.
- 44. Pye, J., & White, A. (2014). Self-mixing in single-tank molten salt TES systems: Mechanisms and mitigation. *Solar Energy*, 103, 196–210.

- 45. Reddy, K. S., & Kaushik, S. C. (2013). Solar thermal power plant performance analysis with stratified TES. *Energy Conversion and Management*, 66, 273–284.
- 46. Pacheco, J. E., Showalter, S. K., & Kolb, W. J. (2002). Development of a molten-salt thermocline thermal storage system. *Journal of Solar Energy Engineering*, 124(2), 153–159.
- 47. Gil, A., Medrano, M., Martorell, I., Lázaro, A., Dolado, P., Zalba, B., & Cabeza, L. F. (2010). State of the art on high-temperature thermal energy storage for power generation. *Renewable and Sustainable Energy Reviews*, 14(1), 31–55.
- 48. Zanganeh, G., Pedretti, A., Zavattoni, S., Barbato, M., & Steinfeld, A. (2013). Packed-bed thermal storage for concentrating solar power Pilot-scale demonstration and industrial-scale design. *Solar Energy*, 86(10), 3084–3098.
- 49. Flueckiger, S. M., Iverson, B. D., Garimella, S. V. (2014). Reducing thermocline degradation in molten-salt thermal storage tanks using flow control strategies. *Journal of Solar Energy Engineering*, 136(4), 041013.
- 50. Misra, R., Saini, J. S., & Saini, R. P. (2013). A review on thermal stratification in hot water storage tanks: Fundamentals and applications. *Renewable and Sustainable Energy Reviews*, 16(5), 3124–3139.
- 51. Pye, J., & White, A. (2014). Optimisation of inlet design for molten salt storage tanks to improve thermal stratification. *Solar Energy*, 103, 236–250.
- 52. Yang, Z., Garimella, S. V., & Srinivasan, R. (2010). Thermal stratification in energy storage tanks: An experimental and numerical study of inlet flow effects. *Applied Energy*, 87(9), 2911–2922.
- 53. Rahimi, M., & Shabani, B. (2017). A review of effective parameters on stratification in thermal storage tanks. *Renewable and Sustainable Energy Reviews*, 69, 1040–1059.
- 54. Libby, C., & Pye, J. (2017). Distributed inlet flow control using orifices for thermocline TES tanks: CFD and experimental validation. *Energy Procedia*, 129, 192–199.
- 55. Patankar, S. V. (1980). Numerical Heat Transfer and Fluid Flow. Hemisphere Publishing.

- 56. Bejan, A. (2013). Convection Heat Transfer. John Wiley & Sons.
- 57. Incropera, F. P., DeWitt, D. P., Bergman, T. L., & Lavine, A. S. (2007). Fundamentals of Heat and Mass Transfer. Wiley.
- 58. Cagnoli, M., Froio, A., Savoldi, L., & Zanino, R. (2019). Multi-scale modular analysis of open volumetric receivers for central tower CSP systems. *Solar Energy*, 190, 195–211.
- 59. Hachicha, A. A., Rodríguez, I., & Oliva, A. (2014). CFD modelling of a molten salt thermocline storage tank during the charging process. *Applied Energy*, 123, 47–57.
- 60. Cagnoli, M., Gaggioli, W., Liberatore, R., Russo, V., & Zanino, R. (2023). CFD modelling of an indirect thermocline energy storage prototype for CSP applications. *Solar Energy*, 259, 86–98.
- 61. Flueckiger, S. M., Yang, Z., & Garimella, S. V. (2013). Review of molten-salt thermocline tank modeling for solar thermal energy storage. *Heat Transfer Engineering*, *34*(3), 197–215.